Proceedings of KSAS'03
KSAS 1st International Sessions in 2003 Fall Conference
GyeongJu Korea, November 14-15, 2003

KSAS2003

AERODYNAMIC SHAPE OPTIMIZATION : EXPLORING THE LIMITS OF DESIGN

Antony Jameson
Department of Aeronautics and Astronautics
Stanford University
jameson@baboon.stanford.edu

Prepared with the assistance of

Sangho Kim
Department of Aeronautics and Astronautics
Stanford University
sangho@stanford.edu

Sriram Shankaran
Department of Aeronautics and Astronautics
Stanford University
ssriram@stanford.edu

Kasidit Leoviriyakit
Department of Aeronautics and Astronautics
Stanford University
kasidit@stanford.edu

Abstract

This paper discusses the role that computational fluid dynamics (CFD) plays in the design of aircraft. An overview of the design process is provided, covering some of the typical decisions that a design team addresses within a multi-disciplinary environment. On a very regular basis trade-offs between disciplines have to be made where a set of conflicting requirements exists. Within an aircraft development project, we focus on the aerodynamic design problem and review how this process has been advanced, first with the improving capabilities of traditional computational fluid dynamics analyses, and then with aerodynamic optimizations based on these increasingly accurate methods.

1 Background

The past 25 years have seen a revolution in the entire engineering design process as computational simulation has come to play an increasingly dominant role. Most notably, computer aided design (CAD) methods have essentially replaced the drawing board as the basic tool for the definition and control of the configuration. Computer visualization techniques enable the designer to verify that no interferences exist between different parts in the layout.

Similarly, structural analysis is now almost entirely carried out by computational methods, typically finite element methods. Commercially available software systems have been progressively developed and augmented with new features, and can treat the full range of requirements for aeronautical structures, including the analysis of stressed skin into the nonlinear range.

The concept of a numerical wind tunnel, which might eventually allow computers "to supplant wind tunnels in the aerodynamic design and testing process", was already a topic of discussion in the 1970-1980. In their celebrated paper of 1975, Chapman, Mark and Pirtle [1] listed three main objective of computational aerodynamics:

1. To provide flow simulations that are either impractical or impossible to obtain in wind tunnels or other ground based experimental test facilities.

2. To lower the time and cost required to obtain aerodynamic flow simulations necessary for the design of new aerospace vehicles.

3. Eventually, to provide more accurate simulations of flight aerodynamics than wind tunnels can.

There have been major advances towards these goals. Despite these, CFD is still not being exploited as effectively as one

would like in the design process. This is partially due to the long set-up time and high costs, both human and computational, associated with complex flow simulations. This paper examines ways to exploit computational simulation more effectively in the overall design process, with the primary focus on aerodynamic design, while recognizing that this should be part of an integrated multi-disciplinary process.

With the availability of high performance computing platforms and robust numerical methods to simulate fluid flows, it is possible to shift attention to automated design procedures which combine CFD with optimization techniques to determine optimum aerodynamic designs. The feasibility of this is by now well established, [2–8] and it is actually possible to calculate optimum three dimensional transonic wing shapes in a few hours, accounting for viscous effects with the flow modeled by the Reynolds averaged Navier-Stokes (RANS) equations. By enforcing constraints on the thickness and span-load distribution one can make sure that there is no penalty in structure weight or fuel volume. Larger scale shape changes such as planform variations can also be accommodated [9]. It then becomes necessary to include a structural weight model to enable a proper compromise between minimum drag and low structure weight to be determined.

Aerodynamic shape optimization has been successfully performed for a variety of complex configurations using multi-block structured meshes [10, 11]. Meshes of this type can be relatively easily deformed to accommodate shape variations required in the redesign. However, it is both extremely time-consuming and expensive in human costs to generate such meshes. Consequently we believe it is essential to develop shape optimization methods which use unstructured meshes for the flow simulation.

Typically, in gradient-based optimization techniques, a control function to be optimized (the wing shape, for example) is parameterized with a set of design variables and a suitable cost function to be minimized is defined. For aerodynamic problems, the cost function is typically lift, drag or a specified target pressure distribution. Then, a constraint, the governing equations can be introduced in order to express the dependence between the cost function and the control function. The sensitivity derivatives of the cost function with respect to the design variables are calculated in order to get a direction of improvement. Finally, a step is taken in this direction and the procedure is repeated until convergence is achieved. Finding a fast and accurate way of calculating the necessary gradient information is essential to developing an effective design method since this can be the most time consuming portion of the design process. This is particularly true in problems which involve a very large number of design variables as is the case in a typical three dimensional shape optimization.

The control theory approach [12–14] has dramatic computational cost advantages over the finite-difference method of calculating gradients. With this approach the necessary gradients are obtained through the solution of an adjoint system of equations of the governing equations of interest. The adjoint method is extremely efficient since the computational expense incurred in the calculation of the complete gradient is effectively independent of the number of design variables.

In the following sections we first examine the fundamental design trade-offs between aerodynamic efficiency and structure weight. Then the design process itself is surveyed in Section 3. We discuss the formulation of shape optimization techniques based on control theory in Section 4–9. In Section 10 we present several case studies which highlight the potential benefits of aerodynamics shape optimization. Finally in Section 11 we suggest some future directions.

2 Aerodynamic Design Trade-offs

Focusing on the design of long range transport aircraft, a good first estimate of performance is provided by the Breguet range equation:

$$Rn = \frac{VL}{D}\frac{1}{E_{sfc}} log \frac{W_0 + W_f}{W_0} = \frac{VL}{D}\frac{1}{E_{sfc}} log \frac{W_1}{W_2}. \qquad (1)$$

Here V is the speed, L/D is the lift to drag ratio, E_{sfc} is the specific fuel consumption of the engines, W_0 is the landing weight(empty weight + payload+ fuel resourced), and W_f is the weight of fuel burnt.

Equation (1) already displays the multi-disciplinary nature of design. A light weight structure is needed to reduce W_0. The specific fuel consumption is mainly the province of the engine manufacturers, and in fact the largest advances in the last 30 years have been in the engine efficiency. The aerodynamic designer should try to maximize VL/D, but must consider the impact of shape modifications on structure weight.

The drag coefficient can be split into an approximately fixed component C_{D_0}, and the induced drag due to lift as

$$C_D = C_{D_0} + \frac{C_L^2}{\pi \varepsilon AR} \qquad (2)$$

where AR is the aspect ratio, and ε is an efficiency factor close to unity. C_{D_0} includes contributions such as friction and form drag. It can be seen from this equation that L/D is maximized by flying at a lift coefficient such that the two terms are equal, so that the induced drag is half the total drag. Moreover, the actual drag

$$D_v = \frac{2L^2}{\pi \varepsilon \rho V^2 b^2}$$

due to lift varies inversely with the square of the span, b. Thus there is a direct conflict between reducing the drag by increasing the span and reducing the structure weight by decreasing it.

It also follows from equation (1) that one should try to maximize VL/D. This means that the cruising speed V should be increased until it approaches the speed of sound C, at which point the formation of shock waves causes the onset of "drag-rise" . Typically the lift to drag ratio will drop from around 19 at a Mach number = V/C in the neighborhood of 0.85, to the order of 4 at Mach 1. Thus the optimum cruise speed will be in the transonic regime, when shock waves are beginning to from , but remain weak enough only to incur a small drag penalty.

The designer can reduce shock drag and delay the onset of drag-rise by increasing the sweep back of the wing or reducing its thickness. Increasing the sweepback increases the structure weight, and may incur problems with stability and control. Decreasing the thickness both reduces the fuel volume (since the wing is used as the main fuel tanks), and increases the structure weight, because for a given stress level in the skin and a given skin thickness, the bending moment that can be supported is directly proportional to the depth of the wing. In the absence of winglets, the optimum span load distribution is elliptic, giving an efficiency factor $\varepsilon = 1$. When, however, the structure weight is taken into account, it is better to shift the load distribution inboard in order to reduce the root bending moment. It may also be necessary to limit the section lift coefficient in the outboard part of the wing, in order to delay the onset of buffet when the lift coefficient is increased to make a turn at a high Mach number.

3 Design Process

The design process can generally be divided into three phases: conceptual design, preliminary design, and final detailed design, as illustrated in Figure 1.

The conceptual design stage defines the mission in the light of anticipated market requirements, and determines a general preliminary configuration capable of performing this mission, together with first estimates of size, weight and performance. A conceptual design requires a staff of 15-30 people. Over a period of 1-2 years, the initial business case is developed. The costs of this phase are the range of 6-12 million dollars, and there is minimal airline involvement

In the preliminary design stage the aerodynamic shape and structural skeleton progress to the point where detailed performance estimates can be made and guaranteed to potential customers, who can then, in turn, formally sign binding contracts for the purchase of a certain number of aircraft. At this stage the development costs are still fairly moderate. A staff of 100-300 people is generally employed for up to 2 years, at a cost of 60-120 million dollars. Initial aerodynamic performance is explored through wind tunnel tests.

In the final design stage the structure must be defined in complete detail, together with complete systems, including the flight deck, control systems (involving major software development for fly-by-wire systems), avionics, electrical and hydraulic systems, landing gear, weapon systems for military aircraft, and cabin layout for commercial aircraft. Major costs are incurred at this stage, during which it is also necessary to prepare a detailed manufacturing plan, together with appropriate facilities and tooling. Thousands of people define every part of the aircraft. Wind Tunnel validation of the final design is carried out. Significant development costs are incurred over a 3 year period, plus an additional year of Flight Testing and Structural Qualification Testing for Certification. Total costs are in the range of 3-12 billion dollars. Thus, the final design would normally be carried out only if sufficient orders have been received to indicate a reasonably high probability of recovering a significant fraction of the investment. For a commercial aircraft there are extensive discussions with airlines.

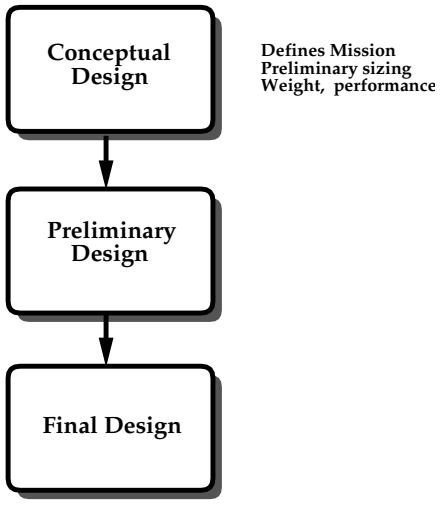

Figure 1. The Overall Design Process

In the development of commercial aircraft, aerodynamic design plays a leading role during the preliminary design stage, during which the definition of the external aerodynamic shape is typically finalized. The aerodynamic lines of the Boeing 777 were frozen, for example, when initial orders were accepted before the initiation of the detailed design of the structure. Figure 2 illustrates the way in which the aerodynamic design process is embedded in the overall preliminary design. The starting point is an initial CAD definition resulting from the conceptual design. The inner loop of aerodynamic analysis is contained in an outer multi-disciplinary loop, which is in turn contained in a major design cycle involving wind tunnel testing. In recent Boeing prac-

tice, three major design cycles, each requiring about 4-6 months, have been used to finalize the wing design. Improvements in CFD which would allow the elimination of a major cycle would significantly shorten the overall design process and therefore reduce costs.

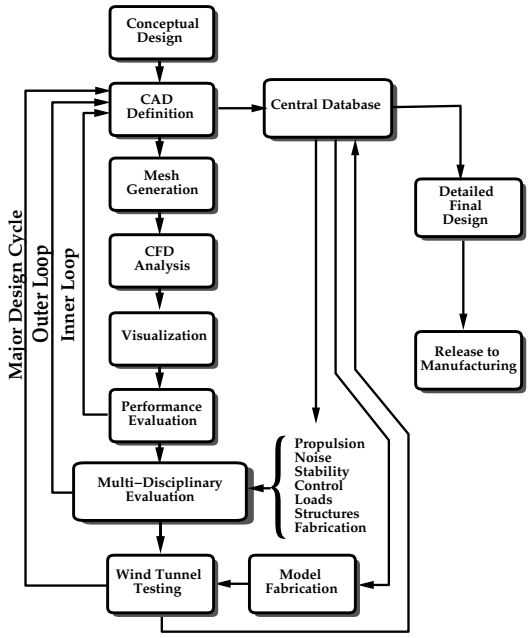

Figure 2. The Aerodynamic Design Process

The inner aerodynamic design loop is used to evaluate numerous variations in the wing definition. In each iteration it is necessary to generate a mesh for the new configuration prior to performing the CFD analysis. Computer graphics software is then used to visualize the results, and the performance is evaluated. The first studies may be confined to partial configurations such as wing-body or wing-body-nacelle combinations. At this stage the focus is on the design of the clean wing. Key points of the flight envelope include the nominal cruise point, cruise at high lift and low lift to allow for the weight variation between the initial and final cruise as the fuel is burned off, and a long range cruise point at lower Mach number, where it is important to ensure there is no significant drag creep. Other defining points are the climb condition, which requires a good lift to drag ratio at low Mach number and high lift coefficient for the clean wing, and buffet conditions. The buffet requirement is typically taken as the high lift cruise point increased to a load of 1.3 g to allow for maneuvering and gust loads.

The aerodynamic analysis interacts with the other disciplines in the next outer loop. These disciplines have their own inner loops, not shown in Figure 2. For an efficient design process the fully updated aero-design database must be accessible to other disciplines without loss of information. For example, the thrust requirements for the power plant design will depend on the drag estimates for take-off, climb and cruise. In order to meet airport noise constraints a rapid climb may be required while the thrust may also be limited. Initial estimates of the lift and moments allow preliminary sizing of the horizontal and vertical tail. This interacts with the design of the control system, where the use of a fly-by-wire system may allow relaxed static stability, hence tail surfaces of reduced size.

First estimates of the aerodynamic loads allow the design of an initial structural skeleton, which in turn provides a weight estimate of the structure. One of the main trade-offs is between aerodynamic performance and wing structure weight. The requirement for fuel volume may also be an important consideration. Manufacturing constraints must also be considered in the final definition of the aerodynamic shape. For example, the curvature in the spanwise direction should be limited. This avoids the need for shot peening which might otherwise be required to produce curvature in both the spanwise and chordwise directions.

From the foregoing considerations, it is apparent that in order to carry out the inner loop of the aerodynamic design process the main requirements for effective CFD software are:

1. Sufficient and known level of accuracy
2. Acceptable computational and manpower costs
3. Fast turn around time

4 Aerodynamic Shape Optimization

Traditionally the process of selecting design variations has been carried out by trial and error, relying on the intuition and experience of the designer. It is also evident that the number of possible design variations is too large to permit their exhaustive evaluation, and thus it is very unlikely that a truly optimum solution can be found without the assistance of automatic optimization procedures. In order to take full advantage of the possibility of examining a large design space, the numerical simulations need to be combined with automatic search and optimization procedures. This can lead to automatic design methods which will fully realize the potential improvements in aerodynamic efficiency.

Ultimately there is a need for multi-disciplinary optimization (MDO), but this can only be effective if it is based on sufficiently high fidelity modeling of the separate disciplines. As a step in this direction there could be significant pay-offs from the application of optimization techniques within the disciplines, where the interactions with other disciplines are taken into account through the introduction of constraints. For example the wing drag can be minimized at a given Mach number and lift

coefficient with a fixed planform, and constraints on minimum thickness to meet requirements for fuel volume and structure weight.

An approach which has become increasingly popular is to carry out a search over a large number of variations via a genetic algorithm. This may allow the discovery of (sometimes unexpected) optimum design choices in very complex multi-objective problems, but it becomes extremely expensive when each evaluation of the cost function requires intensive computation, as is the case in aerodynamic problems.

In order to find optimum aerodynamic shapes with reasonable computational costs, it is useful to regard the wing as a device which controls the flow in order to produce lift with minimum drag. As a result, one can draw on concepts which have been developed in the mathematical theory of control of systems governed by partial differential equations. In particular, an acceptable aerodynamic design must have characteristics that smoothly vary with small changes in shape and flow conditions. Consequently, gradient-based procedures are appropriate for aerodynamic shape optimization. Two main issues affect the efficiency of gradient-based procedures; the first is the actual calculation of the gradient, and the second is the construction of an efficient search procedure which utilizes the gradient.

4.1 Gradient Calculation

For the class of aerodynamic optimization problems under consideration, the design space is essentially infinitely dimensional. Suppose that the performance of a system design can be measured by a cost function I which depends on a function $\mathcal{F}(x)$ that describes the shape, where under a variation of the design, $\delta\mathcal{F}(x)$, the variation of the cost is δI. Now suppose that δI can be expressed to first order as

$$\delta I = \int \mathcal{G}(x)\delta\mathcal{F}(x)dx$$

where $\mathcal{G}(x)$ is the gradient. Then by setting

$$\delta\mathcal{F}(x) = -\lambda\mathcal{G}(x)$$

one obtains an improvement

$$\delta I = -\lambda\int \mathcal{G}^2(x)dx$$

unless $\mathcal{G}(x) = 0$. Thus the vanishing of the gradient is a necessary condition for a local minimum.

Computing the gradient of a cost function for a complex system can be a numerically intensive task, especially if the number of design parameters is large and the cost function is an expensive evaluation. The simplest approach to optimization is to define the geometry through a set of design parameters, which may, for example, be the weights α_i applied to a set of shape functions $\mathcal{B}_i(x)$ so that the shape is represented as

$$\mathcal{F}(x) = \sum \alpha_i \mathcal{B}_i(x).$$

Then a cost function I is selected which might be the drag coefficient or the lift to drag ratio; I is regarded as a function of the parameters α_i. The sensitivities $\frac{\partial I}{\partial \alpha_i}$ may now be estimated by making a small variation $\delta\alpha_i$ in each design parameter in turn and recalculating the flow to obtain the change in I. Then

$$\frac{\partial I}{\partial \alpha_i} \approx \frac{I(\alpha_i + \delta\alpha_i) - I(\alpha_i)}{\delta\alpha_i}.$$

The main disadvantage of this finite-difference approach is that the number of flow calculations needed to estimate the gradient is proportional to the number of design variables [15]. Similarly, if one resorts to direct code differentiation (ADIFOR [16, 17]), or complex-variable perturbations [18], the cost of determining the gradient is also directly proportional to the number of variables used to define the design.

A more cost effective technique is to compute the gradient through the solution of an adjoint problem, such as that developed in references [3, 19, 20]. The essential idea may be summarized as follows. For flow about an arbitrary body, the aerodynamic properties that define the cost function are functions of the flowfield variables (w) and the physical shape of the body, which may be represented by the function $\mathcal{F}$. Then

$$I = I(w, \mathcal{F})$$

and a change in $\mathcal{F}$ results in a change of the cost function

$$\delta I = \frac{\partial I^T}{\partial w}\delta w + \frac{\partial I^T}{\partial \mathcal{F}}\delta\mathcal{F}.$$

Using a technique drawn from control theory, the governing equations of the flowfield are introduced as a constraint in such a way that the final expression for the gradient does not require reevaluation of the flowfield. In order to achieve this, δw must be eliminated from the above equation. Suppose that the governing equation R, which expresses the dependence of w and $\mathcal{F}$ within the flowfield domain D, can be written as

$$R(w, \mathcal{F}) = 0. \tag{3}$$

Then δw is determined from the equation

$$\delta R = \left[\frac{\partial R}{\partial w}\right] \delta w + \left[\frac{\partial R}{\partial \mathcal{F}}\right] \delta \mathcal{F} = 0.$$

Next, introducing a Lagrange multiplier ψ, we have

$$\delta I = \frac{\partial I^T}{\partial w}\delta w + \frac{\partial I^T}{\partial \mathcal{F}}\delta \mathcal{F} - \psi^T \left(\left[\frac{\partial R}{\partial w}\right] \delta w + \left[\frac{\partial R}{\partial \mathcal{F}}\right] \delta \mathcal{F} \right). \quad (4)$$

With some rearrangement

$$\delta I = \left(\frac{\partial I^T}{\partial w} - \psi^T \left[\frac{\partial R}{\partial w}\right] \right) \delta w + \left(\frac{\partial I^T}{\partial \mathcal{F}} - \psi^T \left[\frac{\partial R}{\partial \mathcal{F}}\right] \right) \delta \mathcal{F}.$$

Choosing ψ to satisfy the adjoint equation

$$\left[\frac{\partial R}{\partial w}\right]^T \psi = \frac{\partial I^T}{\partial w} \quad (5)$$

the term multiplying δw can be eliminated in the variation of the cost function, and we find that

$$\delta I = \mathcal{G} \delta \mathcal{F},$$

where

$$\mathcal{G} = \frac{\partial I^T}{\partial \mathcal{F}} - \psi^T \left[\frac{\partial R}{\partial \mathcal{F}}\right].$$

The advantage is that the variation in cost function is independent of δw, with the result that the gradient of I with respect to any number of design variables can be determined without the need for additional flow-field evaluations.

In the case that (3) is a partial differential equation, the adjoint equation (5) is also a partial differential equation and appropriate boundary conditions must be determined. It turns out that the appropriate boundary conditions depend on the choice of the cost function, and may easily be derived for cost functions that involve surface-pressure integrations. Cost functions involving field integrals lead to the appearance of a source term in the adjoint equation.

The cost of solving the adjoint equation is comparable to that of solving the flow equation. Hence, the cost of obtaining the gradient is comparable to the cost of two function evaluations, regardless of the dimension of the design space.

5 Design using the Euler Equations

The application of control theory to aerodynamic design problems is illustrated in this section for the case of three-dimensional wing design using the compressible Euler equations as the mathematical model. The extension of the method to treat the Navier-Stokes equations is presented in references [4, 8, 21]. It proves convenient to denote the Cartesian coordinates and velocity components by x_1, x_2, x_3 and u_1, u_2, u_3, and to use the convention that summation over $i = 1$ to 3 is implied by a repeated index i. Then, the three-dimensional Euler equations may be written as

$$\frac{\partial w}{\partial t} + \frac{\partial f_i}{\partial x_i} = 0 \quad \text{in } D, \quad (6)$$

where

$$w = \begin{Bmatrix} \rho \\ \rho u_1 \\ \rho u_2 \\ \rho u_3 \\ \rho E \end{Bmatrix}, \quad f_i = \begin{Bmatrix} \rho u_i \\ \rho u_i u_1 + p\delta_{i1} \\ \rho u_i u_2 + p\delta_{i2} \\ \rho u_i u_3 + p\delta_{i3} \\ \rho u_i H \end{Bmatrix} \quad (7)$$

and δ_{ij} is the Kronecker delta function. Also,

$$p = (\gamma - 1)\rho \left\{ E - \frac{1}{2}(u_i u_i) \right\}, \quad (8)$$

and

$$\rho H = \rho E + p \quad (9)$$

where γ is the ratio of the specific heats.

In order to simplify the derivation of the adjoint equations, we map the solution to a fixed computational domain with coordinates ξ_1, ξ_2, ξ_3 where

$$K_{ij} = \left[\frac{\partial x_i}{\partial \xi_j}\right], \quad J = \det(K), \quad K^{-1}_{ij} = \left[\frac{\partial \xi_i}{\partial x_j}\right],$$

and

$$S = JK^{-1}.$$

The elements of S are the cofactors of K, and in a finite volume discretization they are just the face areas of the computational cells projected in the x_1, x_2, and x_3 directions. Using the permutation tensor ε_{ijk} we can express the elements of S as

$$S_{ij} = \frac{1}{2}\varepsilon_{jpq}\varepsilon_{irs}\frac{\partial x_p}{\partial \xi_r}\frac{\partial x_q}{\partial \xi_s}. \tag{10}$$

Then

$$\begin{aligned}\frac{\partial}{\partial \xi_i}S_{ij} &= \frac{1}{2}\varepsilon_{jpq}\varepsilon_{irs}\left(\frac{\partial^2 x_p}{\partial \xi_r \partial \xi_i}\frac{\partial x_q}{\partial \xi_s} + \frac{\partial x_p}{\partial \xi_r}\frac{\partial^2 x_q}{\partial \xi_s \partial \xi_i}\right)\\ &= 0.\end{aligned} \tag{11}$$

Also in the subsequent analysis of the effect of a shape variation it is useful to note that

$$\begin{aligned}S_{1j} &= \varepsilon_{jpq}\frac{\partial x_p}{\partial \xi_2}\frac{\partial x_q}{\partial \xi_3},\\ S_{2j} &= \varepsilon_{jpq}\frac{\partial x_p}{\partial \xi_3}\frac{\partial x_q}{\partial \xi_1},\\ S_{3j} &= \varepsilon_{jpq}\frac{\partial x_p}{\partial \xi_1}\frac{\partial x_q}{\partial \xi_2}.\end{aligned} \tag{12}$$

Now, multiplying equation(6) by J and applying the chain rule,

$$J\frac{\partial w}{\partial t} + R(w) = 0 \tag{13}$$

where

$$R(w) = S_{ij}\frac{\partial f_j}{\partial \xi_i} = \frac{\partial}{\partial \xi_i}(S_{ij}f_j), \tag{14}$$

using (11). We can write the transformed fluxes in terms of the scaled contravariant velocity components

$$U_i = S_{ij}u_j$$

as

$$F_i = S_{ij}f_j = \begin{bmatrix}\rho U_i\\ \rho U_i u_1 + S_{i1}p\\ \rho U_i u_2 + S_{i2}p\\ \rho U_i u_3 + S_{i3}p\\ \rho U_i H\end{bmatrix}.$$

For convenience, the coordinates ξ_i describing the fixed computational domain are chosen so that each boundary conforms to a constant value of one of these coordinates. Variations in the shape then result in corresponding variations in the mapping derivatives defined by K_{ij}. Suppose that the performance is measured by a cost function

$$I = \int_{\mathcal{B}} \mathcal{M}(w,S)\,dB_\xi + \int_{\mathcal{D}} \mathcal{P}(w,S)\,dD_\xi,$$

containing both boundary and field contributions where dB_ξ and dD_ξ are the surface and volume elements in the computational domain. In general, $\mathcal{M}$ and $\mathcal{P}$ will depend on both the flow variables w and the metrics S defining the computational space. The design problem is now treated as a control problem where the boundary shape represents the control function, which is chosen to minimize I subject to the constraints defined by the flow equations (13). A shape change produces a variation in the flow solution δw and the metrics δS which in turn produce a variation in the cost function

$$\delta I = \int_{\mathcal{B}} \delta\mathcal{M}(w,S)\,dB_\xi + \int_{\mathcal{D}} \delta\mathcal{P}(w,S)\,dD_\xi. \tag{15}$$

This can be split as

$$\delta I = \delta I_I + \delta I_{II}, \tag{16}$$

with

$$\begin{aligned}\delta\mathcal{M} &= [\mathcal{M}_w]_I\,\delta w + \delta\mathcal{M}_{II},\\ \delta\mathcal{P} &= [\mathcal{P}_w]_I\,\delta w + \delta\mathcal{P}_{II},\end{aligned} \tag{17}$$

where we continue to use the subscripts I and II to distinguish between the contributions associated with the variation of the flow solution δw and those associated with the metric variations δS. Thus $[\mathcal{M}_w]_I$ and $[\mathcal{P}_w]_I$ represent $\frac{\partial \mathcal{M}}{\partial w}$ and $\frac{\partial \mathcal{P}}{\partial w}$ with the metrics fixed, while $\delta\mathcal{M}_{II}$ and $\delta\mathcal{P}_{II}$ represent the contribution of the metric variations δS to $\delta\mathcal{M}$ and $\delta\mathcal{P}$.

In the steady state, the constraint equation (13) specifies the variation of the state vector δw by

$$\delta R = \frac{\partial}{\partial \xi_i}\delta F_i = 0. \tag{18}$$

Here also, δR and δF_i can be split into contributions associated with δw and δS using the notation

$$\begin{aligned}\delta R &= \delta R_I + \delta R_{II}\\ \delta F_i &= [F_{iw}]_I\,\delta w + \delta F_{iII}.\end{aligned} \tag{19}$$

where

$$[F_{i_w}]_I = S_{ij}\frac{\partial f_i}{\partial w}.$$

Multiplying by a co-state vector ψ, which will play an analogous role to the Lagrange multiplier introduced in equation (4), and integrating over the domain produces

$$\int_{\mathcal{D}} \psi^T \frac{\partial}{\partial \xi_i}\delta F_i d\mathcal{D}_\xi = 0. \tag{20}$$

Assuming that ψ is differentiable, the terms with subscript I may be integrated by parts to give

$$\int_{\mathcal{B}} n_i \psi^T \delta F_{i_I} d\mathcal{B}_\xi - \int_{\mathcal{D}} \frac{\partial \psi^T}{\partial \xi_i}\delta F_{i_I} d\mathcal{D}_\xi + \int_{\mathcal{D}} \psi^T \delta R_{II} d\mathcal{D}_\xi = 0. \tag{21}$$

This equation results directly from taking the variation of the weak form of the flow equations, where ψ is taken to be an arbitrary differentiable test function. Since the left hand expression equals zero, it may be subtracted from the variation in the cost function (15) to give

$$\begin{aligned}\delta I = \delta I_{II} &- \int_{\mathcal{D}} \psi^T \delta R_{II} d\mathcal{D}_\xi + \int_{\mathcal{B}} \left[\delta \mathcal{M}_I - n_i \psi^T \delta F_{i_I}\right] d\mathcal{B}_\xi \\ &+ \int_{\mathcal{D}} \left[\delta \mathcal{P}_I + \frac{\partial \psi^T}{\partial \xi_i}\delta F_{i_I}\right] d\mathcal{D}_\xi.\end{aligned} \tag{22}$$

Now, since ψ is an arbitrary differentiable function, it may be chosen in such a way that δI no longer depends explicitly on the variation of the state vector δw. The gradient of the cost function can then be evaluated directly from the metric variations without having to recompute the variation δw resulting from the perturbation of each design variable.

Comparing equations (17) and (19), the variation δw may be eliminated from (22) by equating all field terms with subscript "I" to produce a differential adjoint system governing ψ

$$\frac{\partial \psi^T}{\partial \xi_i}[F_{i_w}]_I + [\mathcal{P}_w]_I = 0 \quad \text{in } \mathcal{D}. \tag{23}$$

Taking the transpose of equation (23), in the case that there is no field integral in the cost function, the inviscid adjoint equation may be written as

$$C_i^T \frac{\partial \psi}{\partial \xi_i} = 0 \quad \text{in } \mathcal{D}, \tag{24}$$

where the inviscid Jacobian matrices in the transformed space are given by

$$C_i = S_{ij}\frac{\partial f_j}{\partial w}.$$

The corresponding adjoint boundary condition is produced by equating the subscript "I" boundary terms in equation (22) to produce

$$n_i \psi^T [F_{i_w}]_I = [\mathcal{M}_w]_I \quad \text{on } \mathcal{B}. \tag{25}$$

The remaining terms from equation (22) then yield a simplified expression for the variation of the cost function which defines the gradient

$$\delta I = \delta I_{II} - \int_{\mathcal{D}} \psi^T \delta R_{II} d\mathcal{D}_\xi, \tag{26}$$

which consists purely of the terms containing variations in the metrics, with the flow solution fixed. Hence an explicit formula for the gradient can be derived once the relationship between mesh perturbations and shape variations is defined.

The boundary conditions satisfied by the flow equations restrict the form of the left hand side of the adjoint boundary condition (25). Consequently, the boundary contribution to the cost function $\mathcal{M}$ cannot be specified arbitrarily. Instead, it must be chosen from the class of functions which allow cancellation of all terms containing δw in the boundary integral of equation (22). On the other hand, there is no such restriction on the specification of the field contribution to the cost function $\mathcal{P}$, since these terms may always be absorbed into the adjoint field equation (23) as source terms.

For simplicity, it will be assumed that the portion of the boundary that undergoes shape modifications is restricted to the coordinate surface $\xi_2 = 0$. Then equations (22) and (25) may be simplified by incorporating the conditions

$$n_1 = n_3 = 0, \quad n_2 = 1, \quad d\mathcal{B}_\xi = d\xi_1 d\xi_3,$$

so that only the variation δF_2 needs to be considered at the wall boundary. The condition that there is no flow through the wall boundary at $\xi_2 = 0$ is equivalent to

$$U_2 = 0,$$

so that

$$\delta U_2 = 0$$

when the boundary shape is modified. Consequently the variation of the inviscid flux at the boundary reduces to

$$\delta F_2 = \delta p \begin{Bmatrix} 0 \\ S_{21} \\ S_{22} \\ S_{23} \\ 0 \end{Bmatrix} + p \begin{Bmatrix} 0 \\ \delta S_{21} \\ \delta S_{22} \\ \delta S_{23} \\ 0 \end{Bmatrix}. \tag{27}$$

Since δF_2 depends only on the pressure, it is now clear that the performance measure on the boundary $\mathcal{M}(w,S)$ may only be a function of the pressure and metric terms. Otherwise, complete cancellation of the terms containing δw in the boundary integral would be impossible. One may, for example, include arbitrary measures of the forces and moments in the cost function, since these are functions of the surface pressure.

In order to design a shape which will lead to a desired pressure distribution, a natural choice is to set

$$I = \frac{1}{2}\int_{\mathcal{B}} (p - p_d)^2 \, dS$$

where p_d is the desired surface pressure, and the integral is evaluated over the actual surface area. In the computational domain this is transformed to

$$I = \frac{1}{2}\int\int_{\mathcal{B}_w} (p - p_d)^2 \, |S_2| \, d\xi_1 d\xi_3,$$

where the quantity

$$|S_2| = \sqrt{S_{2j} S_{2j}}$$

denotes the face area corresponding to a unit element of face area in the computational domain. Now, to cancel the dependence of the boundary integral on δp, the adjoint boundary condition reduces to

$$\psi_j n_j = p - p_d \tag{28}$$

where n_j are the components of the surface normal

$$n_j = \frac{S_{2j}}{|S_2|}.$$

This amounts to a transpiration boundary condition on the costate variables corresponding to the momentum components. Note that it imposes no restriction on the tangential component of ψ at the boundary.

We find finally that

$$\delta I = -\int_{\mathcal{D}} \frac{\partial \psi^T}{\partial \xi_i} \delta S_{ij} f_j \, d\mathcal{D} - \int\int_{B_W} (\delta S_{21}\psi_2 + \delta S_{22}\psi_3 + \delta S_{23}\psi_4)\, p \, d\xi_1 d\xi_3. \tag{29}$$

Here the expression for the cost variation depends on the mesh variations throughout the domain which appear in the field integral. However, the true gradient for a shape variation should not depend on the way in which the mesh is deformed, but only on the true flow solution. In the next section we show how the field integral can be eliminated to produce a reduced gradient formula which depends only on the boundary movement.

6 The Reduced Gradient Formulation

Consider the case of a mesh variation with a fixed boundary. Then,

$$\delta I = 0$$

but there is a variation in the transformed flux,

$$\delta F_i = C_i \delta w + \delta S_{ij} f_j.$$

Here the true solution is unchanged. Thus, the variation δw is due to the mesh movement δx at each mesh point. Therefore

$$\delta w = \nabla w \cdot \delta x = \frac{\partial w}{\partial x_j} \delta x_j \, (= \delta w^*)$$

and since

$$\frac{\partial}{\partial \xi_i} \delta F_i = 0,$$

it follows that

$$\frac{\partial}{\partial \xi_i} (\delta S_{ij} f_j) = -\frac{\partial}{\partial \xi_i} (C_i \delta w^*). \tag{30}$$

It is verified in the following paragraph that this relation holds in the general case with boundary movement. Now

$$\begin{aligned}\int_{\mathcal{D}} \psi^T \delta R d\mathcal{D} &= \int_{\mathcal{D}} \psi^T \frac{\partial}{\partial \xi_i} C_i \left(\delta w - \delta w^*\right) d\mathcal{D} \\ &= \int_{\mathcal{B}} \psi^T C_i \left(\delta w - \delta w^*\right) d\mathcal{B} \\ &- \int_{\mathcal{D}} \frac{\partial \psi^T}{\partial \xi_i} C_i \left(\delta w - \delta w^*\right) d\mathcal{D}. \end{aligned} \tag{31}$$

Here on the wall boundary

$$C_2 \delta w = \delta F_2 - \delta S_{2j} f_j. \tag{32}$$

Thus, by choosing ψ to satisfy the adjoint equation (24) and the adjoint boundary condition (25), we reduce the cost variation to a boundary integral which depends only on the surface displacement:

$$\begin{aligned}\delta I = &\int_{\mathcal{B}_W} \psi^T \left(\delta S_{2j} f_j + C_2 \delta w^*\right) d\xi_1 d\xi_3 \\ &-\iint_{B_W} \left(\delta S_{21}\psi_2 + \delta S_{22}\psi_3 + \delta S_{23}\psi_4\right) p \, d\xi_1 d\xi_3. \end{aligned} \tag{33}$$

For completeness the general derivation of equation (30) is presented here. Using the formula (10), and the property (11)

$$\begin{aligned}&\tfrac{\partial}{\partial \xi_i}\left(\delta S_{ij} f_j\right) \\ &= \frac{1}{2}\frac{\partial}{\partial \xi_i}\left\{\varepsilon_{jpq}\varepsilon_{irs}\left(\frac{\partial \delta x_p}{\partial \xi_r}\frac{\partial x_q}{\partial \xi_s} + \frac{\partial x_p}{\partial \xi_r}\frac{\partial \delta x_q}{\partial \xi_s}\right) f_j\right\} \\ &= \frac{1}{2}\varepsilon_{jpq}\varepsilon_{irs}\left(\frac{\partial \delta x_p}{\partial \xi_r}\frac{\partial x_q}{\partial \xi_s} + \frac{\partial x_p}{\partial \xi_r}\frac{\partial \delta x_q}{\partial \xi_s}\right)\frac{\partial f_j}{\partial \xi_i} \\ &= \frac{1}{2}\varepsilon_{jpq}\varepsilon_{irs}\left\{\frac{\partial}{\partial \xi_r}\left(\delta x_p \frac{\partial x_q}{\partial \xi_s}\frac{\partial f_j}{\partial \xi_i}\right)\right\} \\ &+ \frac{1}{2}\varepsilon_{jpq}\varepsilon_{irs}\left\{\frac{\partial}{\partial \xi_s}\left(\delta x_q \frac{\partial x_p}{\partial \xi_r}\frac{\partial f_j}{\partial \xi_i}\right)\right\} \\ &= \frac{\partial}{\partial \xi_r}\left(\delta x_p \varepsilon_{pqj}\varepsilon_{rsi}\frac{\partial x_q}{\partial \xi_s}\frac{\partial f_j}{\partial \xi_i}\right). \end{aligned} \tag{34}$$

Now express δx_p in terms of a shift in the original computational coordinates

$$\delta x_p = \frac{\partial x_p}{\partial \xi_k}\delta \xi_k.$$

Then we obtain

$$\frac{\partial}{\partial \xi_i}\left(\delta S_{ij} f_j\right) = \frac{\partial}{\partial \xi_r}\left(\varepsilon_{pqj}\varepsilon_{rsi}\frac{\partial x_p}{\partial \xi_k}\frac{\partial x_q}{\partial \xi_s}\frac{\partial f_j}{\partial \xi_i}\delta \xi_k\right). \tag{35}$$

The term in $\frac{\partial}{\partial \xi_1}$ is

$$\varepsilon_{123}\varepsilon_{pqj}\frac{\partial x_p}{\partial \xi_k}\left(\frac{\partial x_q}{\partial \xi_2}\frac{\partial f_j}{\partial \xi_3} - \frac{\partial x_q}{\partial \xi_3}\frac{\partial f_j}{\partial \xi_2}\right)\delta \xi_k.$$

Here the term multiplying $\delta\xi_1$ is

$$\varepsilon_{jpq}\left(\frac{\partial x_p}{\partial \xi_1}\frac{\partial x_q}{\partial \xi_2}\frac{\partial f_j}{\partial \xi_3} - \frac{\partial x_p}{\partial \xi_1}\frac{\partial x_q}{\partial \xi_3}\frac{\partial f_j}{\partial \xi_2}\right).$$

According to the formulas(12) this may be recognized as

$$S_{2j}\frac{\partial f_1}{\partial \xi_2} + S_{3j}\frac{\partial f_1}{\partial \xi_3}$$

or, using the quasi-linear form(14) of the equation for steady flow, as

$$-S_{1j}\frac{\partial f_1}{\partial \xi_1}.$$

The terms multiplying $\delta\xi_2$ and $\delta\xi_3$ are

$$\varepsilon_{jpq}\left(\frac{\partial x_p}{\partial \xi_2}\frac{\partial x_q}{\partial \xi_2}\frac{\partial f_j}{\partial \xi_3} - \frac{\partial x_p}{\partial \xi_2}\frac{\partial x_q}{\partial \xi_3}\frac{\partial f_j}{\partial \xi_2}\right) = -S_{1j}\frac{\partial f_1}{\partial \xi_2}$$

and

$$\varepsilon_{jpq}\left(\frac{\partial x_p}{\partial \xi_3}\frac{\partial x_q}{\partial \xi_2}\frac{\partial f_j}{\partial \xi_3} - \frac{\partial x_p}{\partial \xi_3}\frac{\partial x_q}{\partial \xi_3}\frac{\partial f_j}{\partial \xi_2}\right) = -S_{1j}\frac{\partial f_1}{\partial \xi_3}.$$

Thus the term in $\frac{\partial}{\partial \xi_1}$ is reduced to

$$-\frac{\partial}{\partial \xi_1}\left(S_{1j}\frac{\partial f_1}{\partial \xi_k}\delta \xi_k\right).$$

Finally, with similar reductions of the terms in $\frac{\partial}{\partial \xi_2}$ and $\frac{\partial}{\partial \xi_3}$, we obtain

$$\frac{\partial}{\partial \xi_i}\left(\delta S_{ij} f_j\right) = -\frac{\partial}{\partial \xi_i}\left(S_{ij}\frac{\partial f_j}{\partial \xi_k}\delta \xi_k\right) = -\frac{\partial}{\partial \xi_i}\left(C_i \delta w^*\right)$$

as was to be proved.

In order to validate the concept, the new gradient equations have been tested for various aerodynamic shape optimization

problems and the accuracy of the gradients using the reduced formula are assessed by comparing with finite-difference gradients, complex-step gradients, and gradients calculated by the previous adjoint method which includes a volume integral [22].

The reduced gradient is crucial for unstructured meshes. If the gradient depends on the form of the mesh modification, then the field integral in the gradient calculation has to be recomputed for mesh modifications corresponding to each design variable. This would be prohibitively expensive if the geometry is treated as a free surface defined by the mesh points. Consequently in order to reduce the computational cost with this approach, the number of design variables would have to be reduced by parameterizing the geometry. However, this reduced set of design variables could not recover all possible shape variations.

7 The Viscous Adjoint Equations

The derivation of the viscous adjoint equations is presented in detail in [21, 23]. Here we summarize the main results, under the assumption that the viscosity and heat conduction coefficients μ and k are essentially independent of the flow, and that their variations may be neglected. This simplification has been successfully used for may aerodynamic problems of interest. However, if the flow variations could result in significant changes in the turbulent viscosity, it may be necessary to account for its variation in the calculation.

7.1 Transformation to Primitive Variables

The formulation of the viscous adjoint terms can be simplified by transforming to the primitive variables

$$\tilde{w}^T = (\rho, u_1, u_2, u_3, p),$$

because the viscous stresses depend on the velocity derivatives $\frac{\partial u_i}{\partial x_j}$, while the heat flux can be expressed as

$$\kappa \frac{\partial}{\partial x_i}\left(\frac{p}{\rho}\right).$$

where $\kappa = \frac{k}{R} = \frac{\gamma\mu}{Pr(\gamma-1)}$. The relationship between the conservative and primitive variations is defined by the expressions

$$\delta w = M\delta\tilde{w}, \quad \delta\tilde{w} = M^{-1}\delta w$$

which make use of the transformation matrices $M = \frac{\partial w}{\partial \tilde{w}}$ and $M^{-1} = \frac{\partial \tilde{w}}{\partial w}$. These matrices are provided in transposed form for future convenience

$$M^T = \begin{bmatrix} 1 & u_1 & u_2 & u_3 & \frac{u_i u_i}{2} \\ 0 & \rho & 0 & 0 & \rho u_1 \\ 0 & 0 & \rho & 0 & \rho u_2 \\ 0 & 0 & 0 & \rho & \rho u_3 \\ 0 & 0 & 0 & 0 & \frac{1}{\gamma-1} \end{bmatrix}$$

$$M^{-1^T} = \begin{bmatrix} 1 & -\frac{u_1}{\rho} & -\frac{u_2}{\rho} & -\frac{u_3}{\rho} & \frac{(\gamma-1)u_i u_i}{2} \\ 0 & \frac{1}{\rho} & 0 & 0 & -(\gamma-1)u_1 \\ 0 & 0 & \frac{1}{\rho} & 0 & -(\gamma-1)u_2 \\ 0 & 0 & 0 & \frac{1}{\rho} & -(\gamma-1)u_3 \\ 0 & 0 & 0 & 0 & \gamma-1 \end{bmatrix}.$$

The conservative and primitive adjoint operators L and $\tilde{L}$ corresponding to the variations δw and $\delta\tilde{w}$ are then related by

$$\int_{\mathcal{D}} \delta w^T L\psi \, d\mathcal{D}_\xi = \int_{\mathcal{D}} \delta\tilde{w}^T \tilde{L}\psi \, d\mathcal{D}_\xi,$$

with

$$\tilde{L} = M^T L,$$

so that after determining the primitive adjoint operator, the conservative operator may be obtained by the transformation $L = M^{-1^T}\tilde{L}$. Since the continuity equation contains no viscous terms, it makes no contribution to the viscous adjoint system. Therefore, the derivation proceeds by first examining the adjoint operators arising from the momentum equations and then the energy equation.

7.2 The Viscous Adjoint Field Operator

In order to make use of the summation convention, it is convenient to set $\psi_{j+1} = \phi_j$ for $j = 1,2,3$ and $\psi_5 = \theta$. Collecting together the contributions from the momentum and energy equations, the viscous adjoint operator in primitive variables can be finally expressed as

$$\begin{aligned}
(\tilde{L}\psi)_1 &= -\tfrac{p}{\rho^2}\tfrac{\partial}{\partial\xi_l}\left(S_{lj}\kappa\tfrac{\partial\theta}{\partial x_j}\right) \\
(\tilde{L}\psi)_{i+1} &= \tfrac{\partial}{\partial\xi_l}\left\{S_{lj}\left[\mu\left(\tfrac{\partial\phi_i}{\partial x_j}+\tfrac{\partial\phi_j}{\partial x_i}\right)+\lambda\delta_{ij}\tfrac{\partial\phi_k}{\partial x_k}\right]\right\} \\
&\quad + \tfrac{\partial}{\partial\xi_l}\left\{S_{lj}\left[\mu\left(u_i\tfrac{\partial\theta}{\partial x_j}+u_j\tfrac{\partial\theta}{\partial x_i}\right)\lambda\delta_{ij}u_k\tfrac{\partial\theta}{\partial x_k}\right]\right\} \\
&\quad - \sigma_{ij}S_{lj}\tfrac{\partial\theta}{\partial\xi_l} \qquad \text{for} \quad i = 1,2,3 \\
(\tilde{L}\psi)_5 &= \tfrac{1}{\rho}\tfrac{\partial}{\partial\xi_l}\left(S_{lj}\kappa\tfrac{\partial\theta}{\partial x_j}\right).
\end{aligned}$$

The conservative viscous adjoint operator may now be obtained by the transformation

$$L = M^{-1^T} \tilde{L}.$$

7.3 Boundary Conditions for Force Optimization

Defining the components of the total surface stress as

$$\tau_k = n_j \left(\delta_{kj} p + \sigma_{kj} \right)$$

and the physical surface element

$$dS = |S_2| \, d\mathcal{B}_\xi,$$

the force in a direction with cosines q_i has the form

$$C_q = \int_{\mathcal{B}} q_i \tau_i dS.$$

Integrating the field terms by parts, cancellation with the flow variation terms mandates the adjoint boundary condition

$$\phi_k = q_k.$$

7.4 Boundary Conditions for Inverse Design

In the case of high Reynolds number, the boundary condition for inverse design is well approximated by the equations

$$\phi_k = n_k \left(p - p_d \right), \tag{36}$$

which should be compared with the single scalar equation derived for the inviscid boundary condition (28).

The inviscid boundary condition (28) is satisfied by equation (36), but this represents an over-specification of the boundary condition since only the single condition (28) needs be specified, corresponding to the slip boundary condition for the inviscid flow equations.

7.5 Boundary Conditions Arising from the Energy Equation

The form of the boundary terms arising from the energy equation depends on the choice of temperature boundary condition at the wall. A natural solution is to set

$$\theta = 0$$

in the constant temperature case or

$$\frac{\partial \theta}{\partial n} = 0$$

in the adiabatic case.

8 Planform Design

The shape changes in wing section needed to improve the transonic wing design are quite small. However, in order to obtain a true optimum design larger scale changes such as changes in the wing planform (sweepback, span, chord, and taper) should be considered. Because these directly affect the structure weight, a meaningful result can only be obtained by considering a cost function that takes account of both the aerodynamic characteristics and the weight.

8.1 Cost Function for Planform Design

In order to design a high performance transonic wing, which will lead to a desired pressure distribution, and to still maintain a realistic shape, the natural choice is to set

$$I = \alpha_1 C_D + \alpha_2 \frac{1}{2} \int_{\mathcal{B}} (p - p_d)^2 dS + \alpha_3 C_W \tag{37}$$

with

$$C_W = \frac{\mathcal{W}_{wing}}{q_\infty S_{ref}} \tag{38}$$

where

C_D	=	drag coefficient,
C_W	=	dimensionless wing structural weight,
p	=	current surface pressure,
p_d	=	desired pressure,
q_∞	=	dynamic pressure,
S_{ref}	=	reference area,
$\mathcal{W}_{wing}$	=	wing structure weight, and
α_1, α_2, α_3	=	weighting parameter for drag, inverse design, and structural weight respectively.

The constant α_2 is introduced to provide the designer some control over the pressure distribution.

A practical way to estimate $\mathcal{W}_{wing}$ is to use the so-called Statistical Group Weights Method, which applies statistical equations based on sophisticated regression analysis. For a cargo/transport wing weight, one can use [24]

$$\mathcal{W}_{weight} = 0.0051 (W_{dg} N_z)^{0.557} S_w^{0.649} A^{0.5} (t/c)_{root}^{-0.4} (1+\lambda)^{0.1} cos(\Lambda)^{-1.0} S_{csw}^{0.1} \tag{39}$$

where

A	=	aspect ratio,
N_z	=	ultimate load factor
	=	1.5 x limit load factor,
S_{csw}	=	control surface area (wing-mounted),
S_w	=	trapezoidal wing area,
t/c	=	thickness to chord ratio,
W_{dg}	=	flight design gross weight,
Λ	=	wing sweep, and
λ	=	taper ratio at 25 % MAC.

In addition, if the wing of interest is modeled by five planform variables such as root chord (c_1), mid-span chord (c_2), tip chord (c_3), span (b), and sweepback(Λ), as shown in Figure 3, the sensitivity of the weight to an individual planform variable can be shown in Figure 4, indicating that the weight increases, as sweepback, span, or chord-length increases.

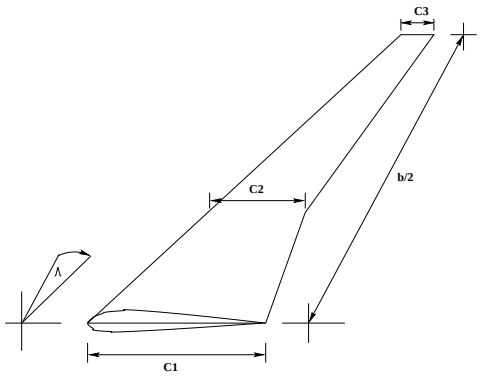

Figure 3. Modeled wing governed by five planform variables; root chord (c_1), mid-span chord (c_2), tip chord (c_3), span (b), and sweepback(Λ).

The increases of sweepback, span, and chord-length affect drag oppositely. As sweepback is increased, the shock drag is weaken. Vortex drag can be reduced by increasing the span.

In these ways the inclusion of a weight estimate in the cost function should prevent the optimization from leading to an unrealistic wing planform, and yield a good overall performance.

8.2 Choice of Weighting Constants

8.2.1 Performance Consideration The choice of α_1 and α_3 greatly affects the optimum shape. An intuitive choice of α_1 and α_3 can be made by considering the problem of maximizing range of an aircraft. Considering the range equation(1) the

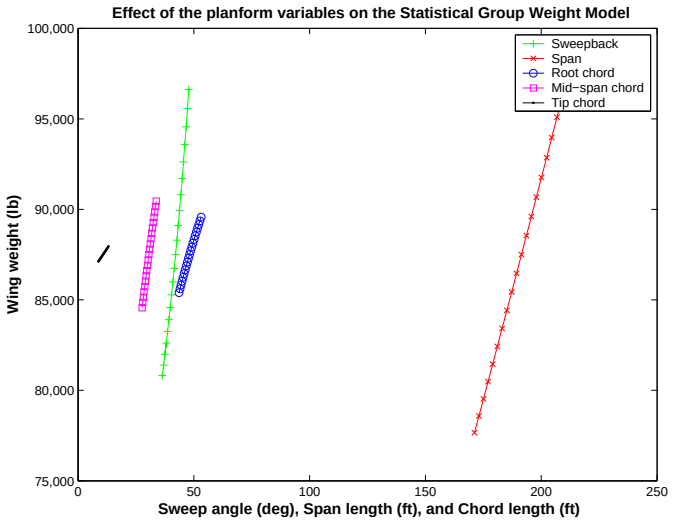

Figure 4. Effect of sweepback(Λ), span (b), root chord(c_1), mid-span chord(c_2), and tip chord(c_3) on the Statistical Group Weights Model

variation of the weight can be expressed as

$$\delta W_2 = \delta W_0 \approx \delta W_{wing}.$$

With fixed $\frac{V}{E_{sfc}}$ and initial weight, W_1, the variation of Range can be stated as

$$\begin{aligned}\delta R_n &= \frac{V}{E_{sfc}}\left(\delta\left(\frac{L}{D}\right) log\frac{W_1}{W_2} + \frac{L}{D}\delta\left(log\frac{W_1}{W_2}\right)\right)\\ &= \frac{V}{E_{sfc}}\left(-\frac{\delta D}{D}\frac{L}{D} log\frac{W_1}{W_2} - \frac{L}{D}\frac{\delta W_2}{W_2}\right)\\ &= -\frac{V}{E_{sfc}}\frac{L}{D} log\frac{W_1}{W_2}\left(\frac{\delta D}{D} + \frac{1}{log\frac{W_1}{W_2}}\frac{\delta W_2}{W_2}\right)\end{aligned}$$

and

$$\begin{aligned}\frac{\delta R_n}{R_n} &= -\left(\frac{\delta C_D}{C_D} + \frac{1}{log\frac{W_1}{W_2}}\frac{\delta W_2}{W_2}\right)\\ &= -\left(\frac{\delta C_D}{C_D} + \frac{1}{log\frac{W_1}{W_2}}\frac{\delta C_W}{\frac{W_2}{q_\infty S_{ref}}}\right).\end{aligned}$$

If we minimize the cost function defined as

$$I = C_D + \alpha C_W,$$

where α is the weighting multiplication, then choosing

$$\alpha = \frac{C_D}{\frac{W_2}{q_\infty S_{ref}} log\frac{W_1}{W_2}}, \tag{40}$$

corresponds to maximizing the range of the aircraft.

8.2.2 Pareto Front In order to present the designer with a wider range of choices, the problem of optimizing both drag and weight can be treated as a multi-objective optimization problem. In this sense one may also view the problem as a "game", where one player tries to minimize C_D and the other tries to minimize C_W. In order to compare the performance of various trial designs, designated by the symbol X in Figure 5, they may be ranked for both drag and weight. A design is undominated if it is impossible either to reduce the drag for the same weight or to reduce the weigth for the same drag. Any dominated point should be eliminated, leaving a set of undominated points which form the Pareto front. In Figure 5, for example, the point Q is dominated by the point P (same drag, less weight) and also the point R (same weight, less drag). So the point Q will be eliminated. The Pareto front can be fit through the points P, R and other dominating points, which may be generated by using an array of different values of α_1 and α_3 in the cost function to compute different optimum shapes. With the aid of the Pareto front the designer will have freedom to pick the most useful design.

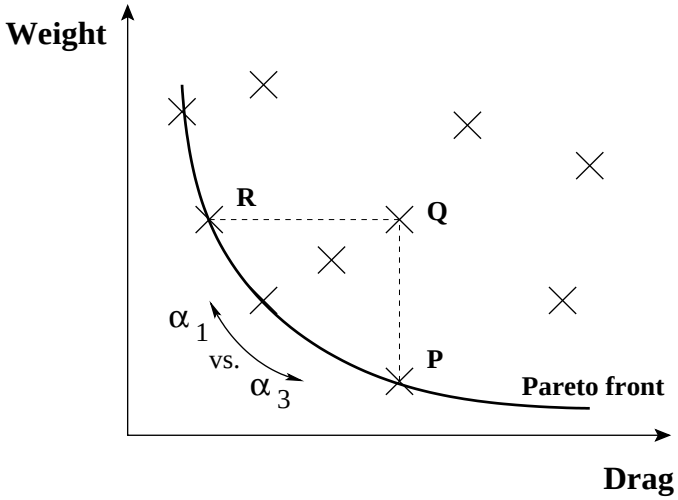

Figure 5. Cooperative game strategy with Drag and Weight as players

9 Optimization Procedure

9.1 The Need for a Sobolev Inner Product in the Definition of the Gradient

Another key issue for successful implementation of the continuous adjoint method is the choice of an appropriate inner product for the definition of the gradient. It turns out that there is an enormous benefit from the use of a modified Sobolev gradient, which enables the generation of a sequence of smooth shapes. This can be illustrated by considering the simplest case of a problem in the calculus of variations.

Suppose that we wish to find the path $y(x)$ which minimizes

$$I = \int_a^b F(y,y')dx$$

with fixed end points $y(a)$ and $y(b)$. Under a variation $\delta y(x)$,

$$\begin{aligned}\delta I &= \int_a^b \left(\frac{\partial F}{\partial y}\delta y + \frac{\partial F}{\partial y'}\delta y'\right) dx \\ &= \int_a^b \left(\frac{\partial F}{\partial y} - \frac{d}{dx}\frac{\partial F}{\partial y'}\right)\delta y dx\end{aligned}$$

Thus defining the gradient as

$$g = \frac{\partial F}{\partial y} - \frac{d}{dx}\frac{\partial F}{\partial y'}$$

and the inner product as

$$(u,v) = \int_a^b uvdx$$

we find that

$$\delta I = (g, \delta y).$$

If we now set

$$\delta y = -\lambda g, \qquad \lambda > 0$$

we obtain a improvement

$$\delta I = -\lambda(g,g) \leq 0$$

unless $g = 0$, the necessary condition for a minimum.

Note that g is a function of y, y', y'',

$$g = g(y, y', y'')$$

In the well known case of the Brachistrone problem, for example, which calls for the determination of the path of quickest descent between two laterally separated points when a particle falls under gravity,

$$F(y, y') = \sqrt{\frac{1+y'^2}{y}}$$

and

$$g = -\frac{1+y'^2+2yy''}{2\left(y(1+y'^2)\right)^{3/2}}$$

It can be seen that each step

$$y^{n+1} = y^n - \lambda^n g^n$$

reduces the smoothness of y by two classes. Thus the computed trajectory becomes less and less smooth, leading to instability.

In order to prevent this we can introduce a weighted Sobolev inner product [25]

$$\langle u, v\rangle = \int (uv + \varepsilon u' v')dx$$

where ε is a parameter that controls the weight of the derivatives. We now define a gradient $\bar{g}$ such that

$$\delta I = \langle \bar{g}, \delta y\rangle$$

Then we have

$$\begin{aligned}\delta I &= \int (\bar{g}\delta y + \varepsilon \bar{g}'\delta y')dx \\ &= \int (\bar{g} - \frac{\partial}{\partial x}\varepsilon\frac{\partial \bar{g}}{\partial x})\delta y dx \\ &= (g, \delta y)\end{aligned}$$

where

$$\bar{g} - \frac{\partial}{\partial x}\varepsilon\frac{\partial \bar{g}}{\partial x} = g$$

and $\bar{g} = 0$ at the end points. Thus $\bar{g}$ can be obtained from g by a smoothing equation. Now the step

$$y^{n+1} = y^n - \lambda^n \bar{g}^n$$

gives an improvement

$$\delta I = -\lambda^n \langle \bar{g}^n, \bar{g}^n\rangle$$

but y^{n+1} has the same smoothness as y^n, resulting in a stable process.

9.2 Sobolev Gradient for Shape Optimization

In applying control theory to aerodynamic shape optimization, the use of a Sobolev gradient is equally important for the preservation of the smoothness class of the redesigned surface. Accordingly, using the weighted Sobolev inner product defined above, we define a modified gradient $\bar{\mathcal{G}}$ such that

$$\delta I = < \bar{\mathcal{G}}, \delta \mathcal{F} > .$$

In the one dimensional case $\bar{\mathcal{G}}$ is obtained by solving the smoothing equation

$$\bar{\mathcal{G}} - \frac{\partial}{\partial \xi_1}\varepsilon\frac{\partial}{\partial \xi_1}\bar{\mathcal{G}} = \mathcal{G}. \tag{41}$$

In the multi-dimensional case the smoothing is applied in product form. Finally we set

$$\delta \mathcal{F} = -\lambda \bar{\mathcal{G}} \tag{42}$$

with the result that

$$\delta I = -\lambda < \bar{\mathcal{G}}, \bar{\mathcal{G}} > \quad < 0,$$

unless $\bar{\mathcal{G}} = 0$, and correspondingly $\mathcal{G} = 0$.

When second-order central differencing is applied to (41), the equation at a given node, i, can be expressed as

$$\bar{\mathcal{G}}_i - \varepsilon\left(\bar{\mathcal{G}}_{i+1} - 2\bar{\mathcal{G}}_i + \bar{\mathcal{G}}_{i-1}\right) = \mathcal{G}_i, \qquad 1 \le i \le n,$$

where $\mathcal{G}_i$ and $\bar{\mathcal{G}}_i$ are the point gradients at node i before and after the smoothing respectively, and n is the number of design variables equal to the number of mesh points in this case. Then,

$$\bar{\mathcal{G}} = A\mathcal{G},$$

where A is the $n \times n$ tri-diagonal matrix such that

$$A^{-1} = \begin{bmatrix} 1+2\varepsilon & -\varepsilon & 0 & . & 0 \\ \varepsilon & . & . & & \\ 0 & . & . & . & \\ . & & . & . & -\varepsilon \\ 0 & & & \varepsilon & 1+2\varepsilon \end{bmatrix} .$$

Using the steepest descent method in each design iteration, a step, $\delta\mathcal{F}$, is taken such that

$$\delta\mathcal{F} = -\lambda A\mathcal{G}. \tag{43}$$

As can be seen from the form of this expression, implicit smoothing may be regarded as a preconditioner which allows the use of much larger steps for the search procedure and leads to a large reduction in the number of design iterations needed for convergence.

9.3 Outline of the Design Procedure

The design procedure can finally be summarized as follows:

1. Solve the flow equations for ρ, u_1, u_2, u_3, p.
2. Solve the adjoint equations for ψ subject to appropriate boundary conditions.
3. Evaluate $\mathcal{G}$ and calculate the corresponding Sobolev gradient $\bar{\mathcal{G}}$.
4. Project $\bar{\mathcal{G}}$ into an allowable subspace that satisfies any geometric constraints.
5. Update the shape based on the direction of steepest descent.
6. Return to 1 until convergence is reached.

Practical implementation of the design method relies heavily upon fast and accurate solvers for both the state (w) and co-state (ψ) systems. The result obtained in Section 10 have been obtained using well-validated software for the solution of the Euler and Navier-Stokes equations developed over the course of many years [26–28]. For inverse design the lift is fixed by the target pressure. In drag minimization it is also appropriate to fix the lift coefficient, because the induced drag is a major fraction of the total drag, and this could be reduced simply by reducing the lift. Therefore the angle of attack is adjusted during each flow solution to force a specified lift coefficient to be attained, and the influence of variations of the angle of attack is included in the calculation of the gradient. The vortex drag also depends on the span loading, which may be constrained by other considerations such as structural loading or buffet onset. Consequently, the option is provided to force the span loading by adjusting the twist distribution as well as the angle of attack during the flow solution.

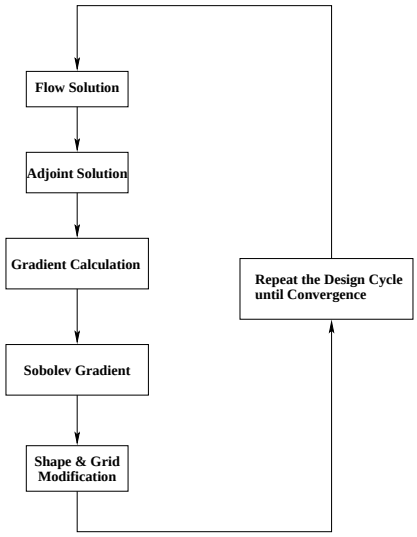

Figure 6. Design cycle

9.4 Computational Costs

In order to address the issue of the search costs, Jameson and Vassberg investigated a variety of techniques in Reference [29] using a trajectory optimization problem (the brachistochrone) as a representative model. The study verified that the search cost (i.e., number of steps) of a simple steepest descent method applied to this problem scales as N^2, where N is the number of design variables, while the cost of quasi-Newton methods scaled linearly with N as expected. On the other hand, with an appropriate amount of smoothing, the smoothed descent method converged in a fixed number of steps, independent of N. Considering that the evaluation of the gradient by a finite difference method requires $N+1$ flow calculations, while the cost of its evaluation by the adjoint method is roughly that of two flow calculations, one arrives at the estimates of total computational cost given in Tables 1-2.

Table 1. Cost of Search Algorithm.

Steepest Descent	$O(N^2)$ steps
Quasi-Newton	$O(N)$ steps
Smoothed Gradient	$O(K)$ steps
(Note: K is independent of N)	

Table 2. Total Computational Cost of Design.

Finite Difference Gradients + Steepest Descent	$O(N^3)$
Finite Difference Gradients + Quasi-Newton Search	$O(N^2)$
Adjoint Gradients + Quasi-Newton Search	$O(N)$
Adjoint Gradients + Smoothed Gradient Search (Note: K is independent of N)	$O(K)$

10 Case Studies

Several design efforts which have utilized these methods include: Raytheon's and Gulfstream business jets, NASA's High-Speed Civil Transport, regional jet designs, as well as several Boeing projects such as the MDXX and the Blended-Wing-Body [30, 31]. Some representative examples of design calculations are presented in this section to illustrate the present capability.

10.1 Viscous Transonic Redesign of the Boeing 747 wing

Over the last decade the adjoint method has been successfully used to refine a variety of designs for flight at both transonic and supersonic cruising speeds. In the case of transonic flight, it is often possible to produce a shock free flow which eliminates the shock drag by making very small changes, typically no larger than the boundary layer displacement thickness. Consequently viscous effects need to be considered in order to realize the full benefits of the optimization.

Here the optimization of the wing of the Boeing 747 is presented to illustrate the kind of benefits that can be obtained. In these calculations the flow was modeled by the Reynolds Averaged Navier-Stokes equations. A Baldwin-Lomax turbulence model was considered sufficient, since the optimization is for the cruise condition with attached flow. The computational mesh is shown in Figure 7.

The calculations were performed to minimize the drag coefficient at a fixed lift coefficient, subject to the additional constraints that the span loading should not be altered and the thickness should not be reduced. It might be possible to reduce the induced drag by modifying the span loading to an elliptic distribution, but this would increase the root bending moment, and consequently require an increase in the skin thickness and structure weight. A reduction in wing thickness would not only reduce the fuel volume, but it would also require an increase in skin thickness to support the bending moment. Thus these constraints assure that there will be no penalty in either structure weight or fuel volume.

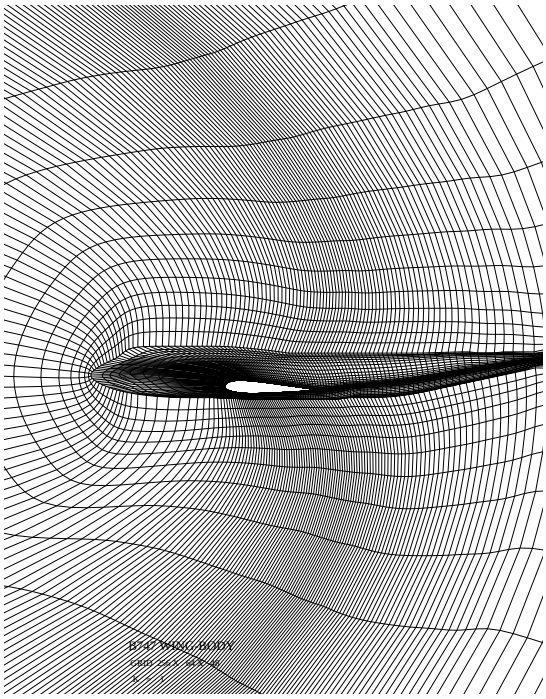

Figure 7. Computational Grid of the B747 Wing Fuselage

Figure 8 displays the result of an optimization at a Mach number of 0.86, which is roughly the maximum cruising Mach number attainable by the existing design before the onset of significant drag rise. The lift coefficient of 0.42 is the contribution of the exposed wing. Allowing for the fuselage, the total lift coefficient is about 0.47. It can be seen that the redesigned wing is essentially shock free, and the drag coefficient is reduced from 0.01269 (127 counts) to 0.01136 (114 counts). The total drag coefficient of the aircraft at this lift coefficient is around 270 counts, so this would represent a drag reduction of the order of 5 percent.

Figure 9 displays the result of an optimization at Mach 0.90. It might be expected that the Boeing 747 wing could be modified to allow an increase in the cruising Mach number because it has a higher sweep-back than later designs, and a rather thin wing section with a thickness to chord ratio of 8 percent. In this case the shock waves are not eliminated, but their strength is significantly weakened, while the drag coefficient is reduced from 0.01819 (182 counts) to 0.01293 (129 counts). Thus the redesigned wing has essentially the same drag at Mach 0.9 as the original wing at Mach 0.86. Figures 10 and 11 verify that the span loading and thickness were not changed by the redesign, while Figures 12 and 13 indicate the required section changes at 42 percent and 68 percent span stations.

10.2 Viscous Planform Redesign of the Boeing 747 wing

We present results to show that the optimization can successfully trade planform parameters. The case chosen is the Boeing 747 wing fuselage combination at Mach 0.90 and a lift coefficient $C_L = 0.42$. We allowed section changes together with variations of sweepback, span, root chord, mid-span chord, and tip chord. Figure 14 shows a baseline calculation with the planform fixed. Here the drag was reduced from 181.9 counts to 127.9 counts (29.7% reduction) in 50 design iterations with relatively small changes in the section shape.

Figure 15 shows the effect of allowing changes in sweepback, span, root chord, mid-span chord, and tip chord. The parameter α_3 was chosen according to formula (40) such that the cost function corresponds to maximizing the range of the aircraft. In 50 design iterations the drag was reduced from 181.9 counts to 124.9 counts (31.3% reduction), while the dimensionless structure weight was slightly increased from 0.02956 to .03047 (3.1% increase). This test case shows a good trade off among the planform variables to achieve an optimal performance for a realistic design. At Mach 0.9, which is an off design point, the drag is quite high. As a result, the optimizer increases the sweepback to weaken shock drag, increases the span to reduce vortex drag, and reduces the thickness to chord ratio (with the thickness fixed) to alleviate shock drag. These changes cause a slight increase of wing weight. But if the wing structural weight is not included in the cost function, the optimal shape will result in an excessive span, chord-length, and sweep angle. As a result of the trade-off between drag reduction and increased wing weight, the overall drag reduction was more than in the previous figure, while the wing weight was slightly increased. These results verify the feasibility of including the effects of planform variations in the optimization.

Figure 16 shows the effect of varying the weighting parameters α_1 and α_3 in the cost function (37). As before the design variables are sweepback, span, chords at three different span locations and mesh points on the wing surface. In Fig. 16 each point corresponds to an optimal shape for one specific choice of (α_1, α_3). By varying α_1 and α_3, we capture the Pareto front which bounds all the non-dominated solutions. All points on this front are acceptable designs in the sense that no improvement can be achieved in one objective that doesn't lead to degradation in the other objective. The optimum shape that corresponds to the optimal Breguet range is also marked in the figure.

Figure 17 shows the change of planform when the $\frac{\alpha_3}{\alpha_1}$ =1. This value of $\frac{\alpha_3}{\alpha_1}$ is sufficient to cause the optimizer to reduce the sweepback, reducing wing weight. But it allows the optimizer to increase the span, reducing vortex drag. This yields an optimum shape which has low structure weight and moderate drag.

10.3 Shape optimization of complete aircraft configurations on unstructured meshes

We have recently extended the adjoint design method to unstructured meshes in order to facilitate the treatment of complete aircraft configurations [32]. Here we take advantage of the reduced gradient formula (33) to reduced the computational cost of the gradient calculation. The results for a transonic business jet are shown below. As shown in Figures 18, 19, 20, 21, the outboard sections of the existing wing have a strong shock while flying at cruise conditions ($M_\infty = 0.80$, $\alpha = 2^o$). The results of a drag minimization that aims to remove the shocks on the wing are shown in Figures 22, 23, 24, 25. The drag has been reduced from 235 counts to 215 counts in about 8 design cycles. The lift was constrained at 0.4 by perturbing the angle of attack. Further, the original thickness of the wing was maintained during the design process ensuring that fuel volume and structural integrity will be maintained by the redesigned shape.

Thickness constraints on the wing were imposed on cutting planes along the span of the wing and by transferring the constrained shape movement back to the nodes of the surface triangulation. The volume mesh was deformed to conform to the shape changes induced using the spring method. The entire design process typically takes about 4 hours on a 1.7 Ghz Athlon processor with 1 Gb of memory. Parallel implementation of the design procedure has also been developed that further reduces the computational cost of this design process.

11 Conclusion

The accumulated experience of the last decade suggests that most existing aircraft which cruise at transonic speeds are amenable to a drag reduction of the order of 3 to 5 percent, or an increase in the drag rise Mach number of at least .02. These improvements can be achieved by very small shape modifications, which are too subtle to allow their determination by trial and error methods. The potential economic benefits are substantial, considering the fuel costs of the entire airline fleet. Moreover, if one were to take full advantage of the increase in the lift to drag ratio during the design process, a smaller aircraft could be designed to perform the same task, resulting in further cost reductions. Consequently we are confident that some methods of this type will provide a basis for aerodynamic designs of the future.

Acknowledgment

This work has benefited greatly from the support of the Air Force Office of Science Research under grant No. AF F49620-98-1-2002.

REFERENCES

[1] D.R. Chapman, H. Mark, and M.W. Pirtle. Computers vs. wind tunnels in aerodynamic flow simulations. *Astronautics and Aeronautics*, 13(4):22–30, 35, 1975.

[2] A. Jameson. Aerodynamic design via control theory. *ICASE Report 88–64, Journal of Scientific Computing*, 3:233–260, 1988.

[3] A. Jameson. Optimum aerodynamic design using control theory. *Computational Fluid Dynamics Review*, pages 495–528, 1995.

[4] A. Jameson and L. Martinelli. Aerodynamic shape optimization techniques based on control theory. Lecture notes in mathematics #1739, proceeding of computational mathematics driven by industrial problems, CIME (International Mathematical Summer (Center), Martina Franca, Italy, June 21-27 1999.

[5] A. Jameson, J. Alonso, J. Reuther, L. Martinelli, and J. Vassberg. Aerodynamic shape optimization techniques based on control theory. *AIAA paper 98-2538*, 29^{th} AIAA Fluid Dynamic Conference, Alburquerque, June 1998.

[6] S. Kim, J. J. Alonso, and A. Jameson. Design optimization of high-lift configurations using a viscous continuous adjoint method. *AIAA paper 2002-0844*, AIAA 40th Aerospace Sciences Meeting & Exhibit, Reno, NV, January 2002.

[7] S. Nadarajah and A. Jameson. Optimal control of unsteady flows using a time accurate method. *AIAA paper 2002-5436*, 9^{th}AIAA/ISSMO Symposium on Multidisciplinary Analysis and Optimization Conference, Atlanta, GA, September 4-6 2002.

[8] A. Jameson, L. Martinelli, and N. A. Pierce. Optimum aerodynamic design using the Navier-Stokes equations. *Theoret. Comput. Fluid Dynamics*, 10:213–237, 1998.

[9] K. Leoviriyakit and A. Jameson. Aerodynamic shape optimization of wings including planform variations. *AIAA paper 2003-0210*, 41^{st} Aerospace Sciences Meeting & Exhibit, Reno, Nevada, January 2003.

[10] J. Reuther, A. Jameson, J. J. Alonso, M. J. Rimlinger, and D. Saunders. Constrained multipoint aerodynamic shape optimization using an adjoint formulation and parallel computers. *AIAA paper 97-0103*, 35th Aerospace Sciences Meeting and Exhibit, Reno, Nevada, January 1997.

[11] S. Cliff, J. Reuther, D. Sanders, and R. Hicks. Single and multipoint aerodynamic shape optimization of high speed civil transport. *Journal of Aircraft*, 38:997–1005, 2001.

[12] J. L. Lions. *Optimal Control of Systems Governed by Partial Differential Equations*. Springer-Verlag, New York, 1971. Translated by S.K. Mitter.

[13] O. Pironneau. *Optimal Shape Design for Elliptic Systems*. Springer-Verlag, New York, 1984.

[14] A. Jameson. *Optimum Aerodynamic Design Using Control Theory, Computational Fluid Dynamics Review 1995*. Wiley, 1995.

[15] R. M. Hicks and P. A. Henne. Wing design by numerical optimization. *Journal of Aircraft*, 15:407–412, 1978.

[16] C. Bischof, A. Carle, G. Corliss, A. Griewank, and P. Hovland. Generating derivative codes from Fortran programs. *Internal report MCS-P263-0991*, Computer Science Division, Argonne National Laboratory and Center of Research on Parallel Computation, Rice University, 1991.

[17] L. L. Green, P. A. Newman, and K. J. Haigler. Sensitivity derivatives for advanced CFD algorithm and viscous modeling parameters via automatic differentiation. *AIAA paper 93-3321*, 11th AIAA Computational Fluid Dynamics Conference, Orlando, Florida, 1993.

[18] W. K. Anderson, J. C. Newman, D. L. Whitfield, and E. J. Nielsen. Sensitivity analysis for the Navier-Stokes equations on unstructured meshes using complex variables. *AIAA paper 99-3294*, Norfolk, VA, June 1999.

[19] A. Jameson. Optimum aerodynamic design using CFD and control theory. *AIAA paper 95-1729*, AIAA 12th Computational Fluid Dynamics Conference, San Diego, CA, June 1995.

[20] A. Jameson, L. Martinelli, J. J. Alonso, J. C. Vassberg, and J. Reuther. Perspectives on simulation based aerodynamic design. In M. Hafez amd K. Morinishi and J. Periauz, editors, *Computational Fluid Dynamics for the 21^{st} Century*, pages 135–178. Notes on Numerical Fluid Dynamics Vol. 78, Springer-Verlag, 2001.

[21] A. Jameson. Aerodynamic shape optimization using the adjoint method. 2002-2003 lecture series at the von karman institute, Von Karman Institute For Fluid Dynamics, Brussels, Belgium, Febuary 3-7 2003.

[22] A. Jameson and S. Kim. Reduction of the adjoint gradient formula in the continuous limit. *AIAA paper 2003-0040*, 41st Aerospace Sciences Meeting & Exhibit, Reno, Nevada, January 2003.

[23] S. Kim. *Design Optimization of High–Lift Configurations Using a Viscous Adjoint-Based Method*. Ph.d. dissertation, Department of Aeronautics and Astronautics, Stanford University, Stanford, CA, August 2001.

[24] Daniel P. Raymer. *Aircraft Design: A Conceptual Approach, Third Edition*. AIAA Education Series, Wright-Patterson Air Force Base, Ohio, 1990.

[25] A. Jameson. Optimum transonic wing design using control theory. Technical report, IUTAM Symposium Transsonicum IV, Goettingen, Germany, September 2–6 2002.

[26] A. Jameson, W. Schmidt, and E. Turkel. Numerical solutions of the Euler equations by finite volume methods with Runge-Kutta time stepping schemes. *AIAA paper 81-1259*, January 1981.

[27] L. Martinelli and A. Jameson. Validation of a multigrid method for the Reynolds averaged equations. *AIAA paper 88-0414*, 1988.

[28] S. Tatsumi, L. Martinelli, and A. Jameson. A new high resolution scheme for compressible viscous flows with shocks. *AIAA paper* To Appear, AIAA 33nd Aerospace Sciences Meeting, Reno, Nevada, January 1995.

[29] A. Jameson and J. C. Vassberg. Studies of alternative numerical optimization methods applied to the brachistochrone problem. In *Proceedings of OptiCON'99*, Newport Beach, CA, October 1999.

[30] R. H. Liebeck. Design of the Blended-Wing-Body subsonic transport. *Wright Brothers Lecture, AIAA paper 2002-0002*, Reno, NV, January 2002.

[31] D. L. Roman, J. B. Allen, and R. H. Liebeck. Aerodynamic design challenges of the Blended-Wing-Body subsonic transport. *AIAA paper 2000-4335*, Denver, CO, August 2000.

[32] A. Jameson, Sriram, and L. Martinelli. An unstructured adjoint method for transonic flows. *AIAA paper*, 16^{th} AIAA CFD Conference, Orlando, FL, June 2003.

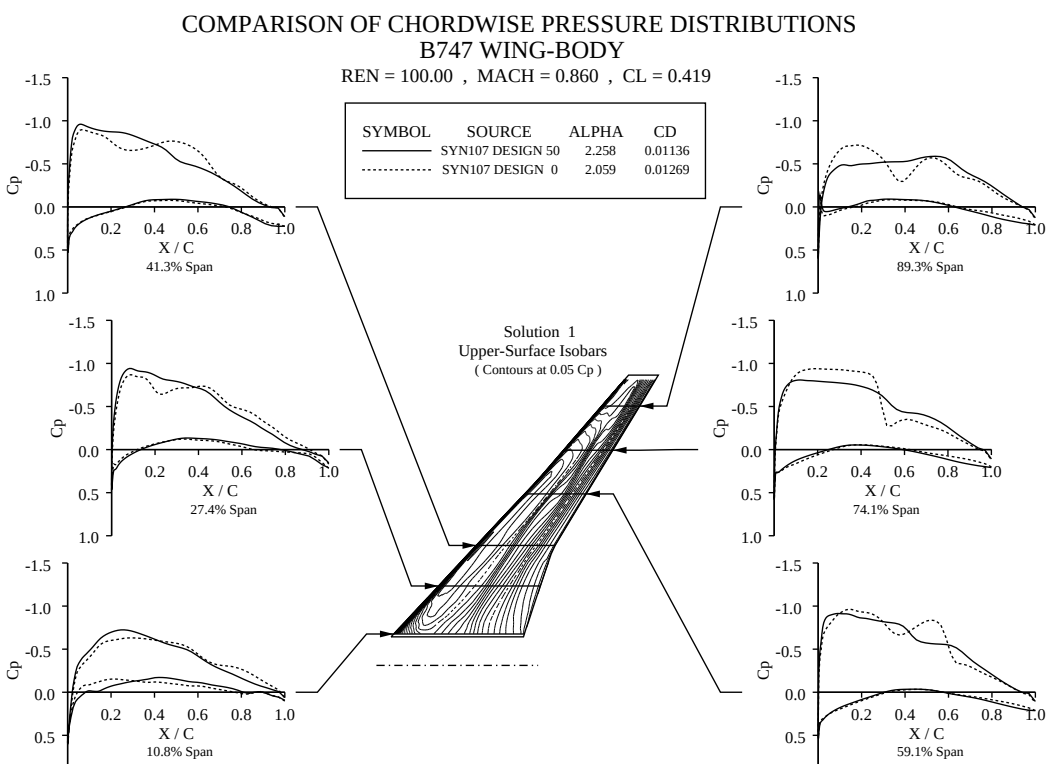

Figure 8. Redesigned Boeing 747 wing at Mach 0.86, Cp distributions

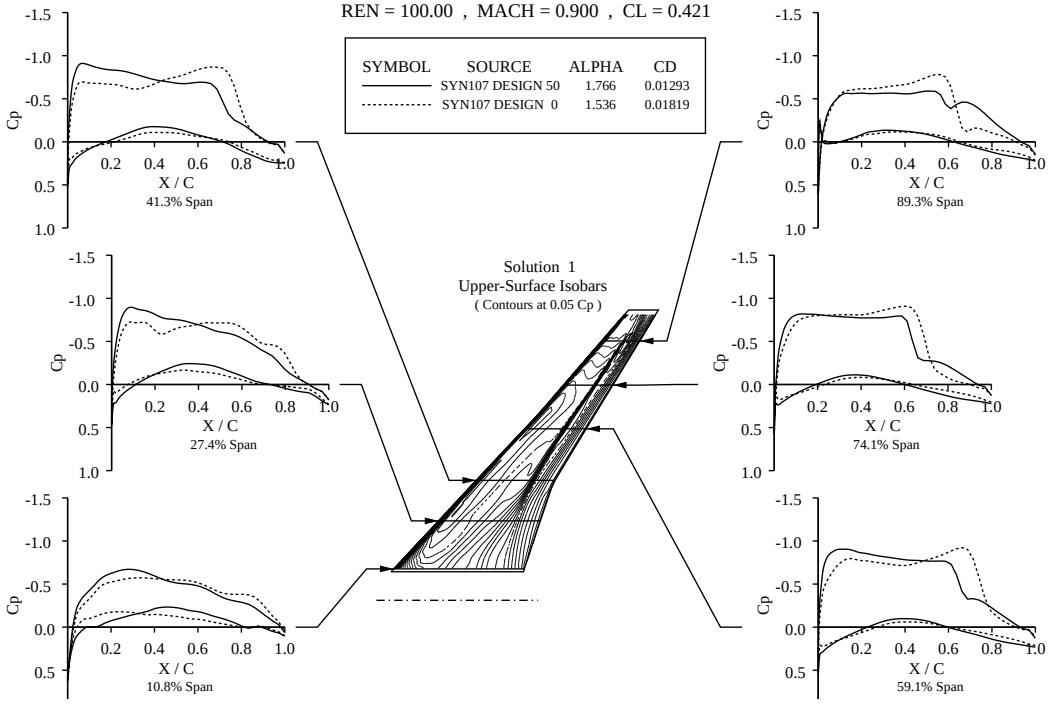

Figure 9. Redesigned Boeing 747 wing at Mach 0.90, Cp distributions

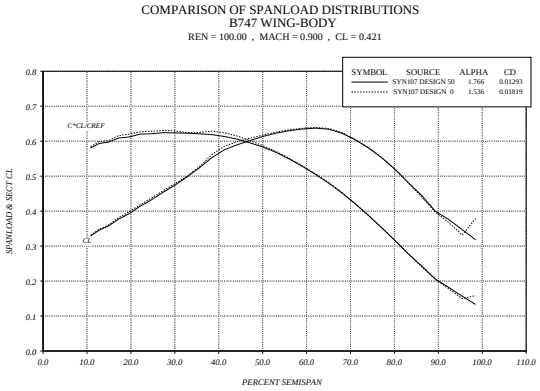

Figure 10. Span loading, Redesigned Boeing 747 wing at Mach 0.90

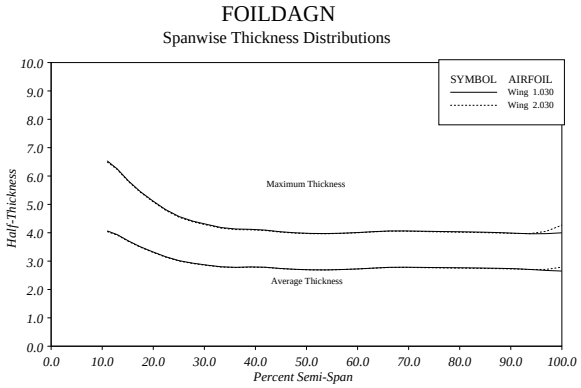

Figure 11. Spanwise thickness distribution, Redesigned Boeing 747 wing at Mach 0.90

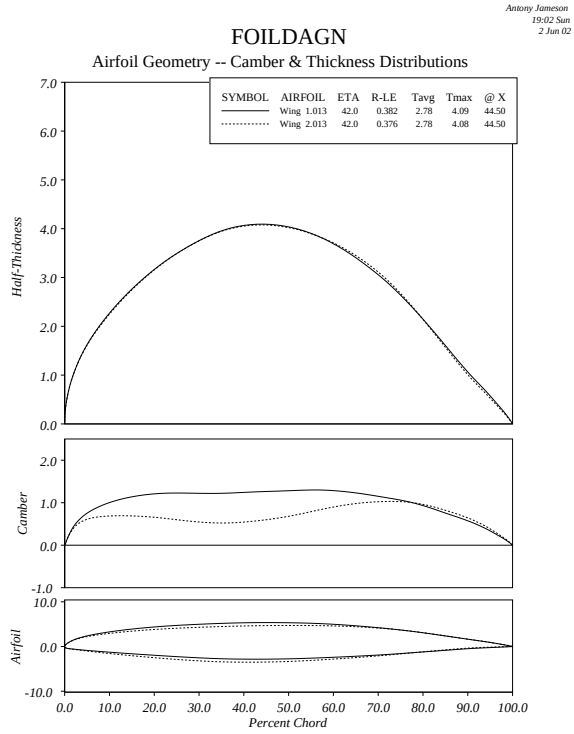

Figure 12. Section geometry at η = 0.42, redesigned Boeing 747 wing at Mach 0.90

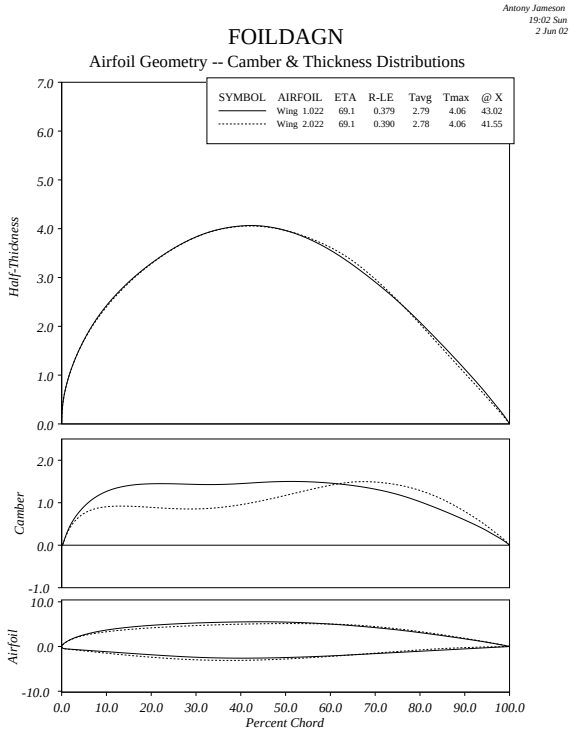

Figure 13. Section geometry at η = 0.68, redesigned Boeing 747 wing at Mach 0.90

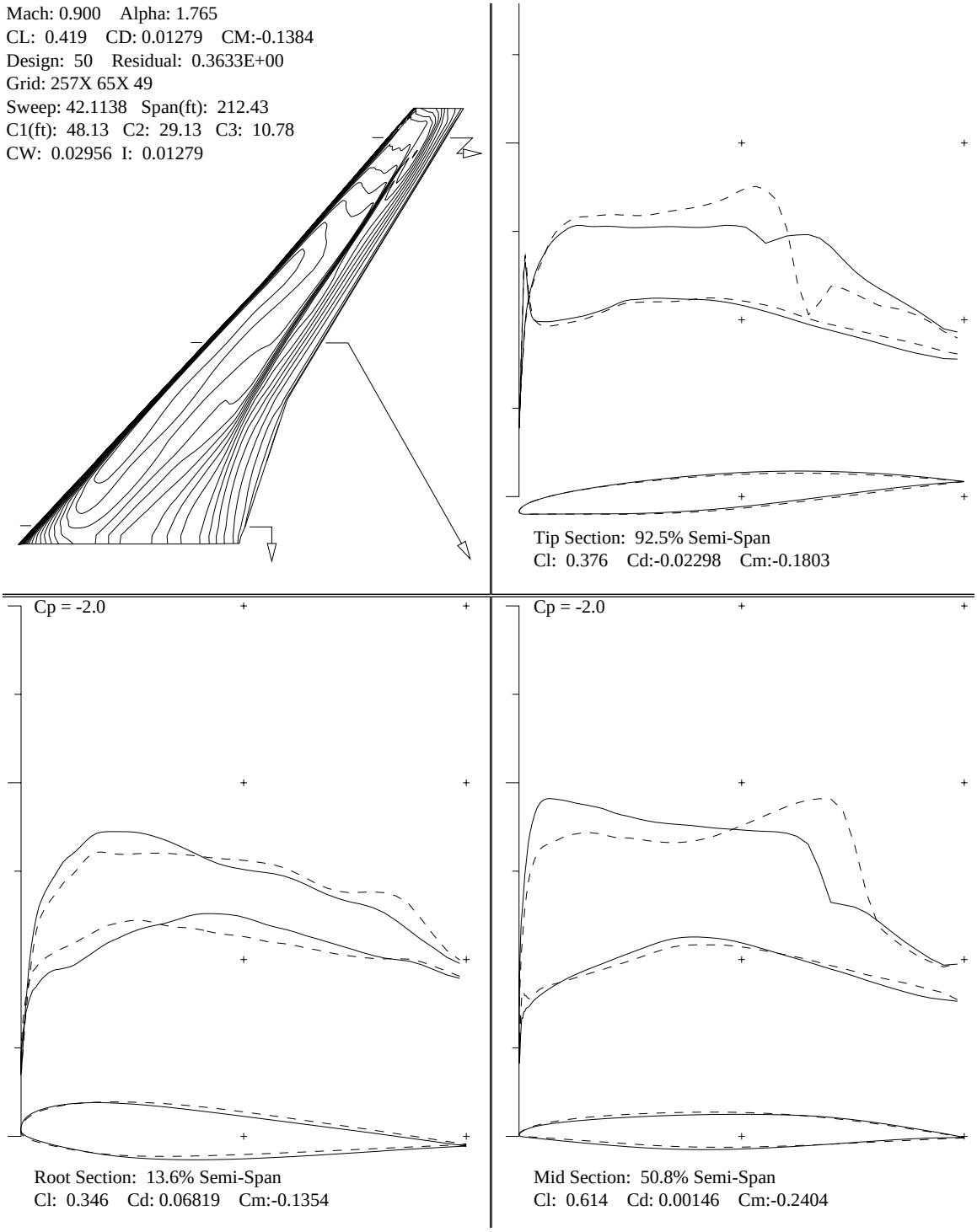

Figure 14. Redesign of Boeing 747, fixed planform

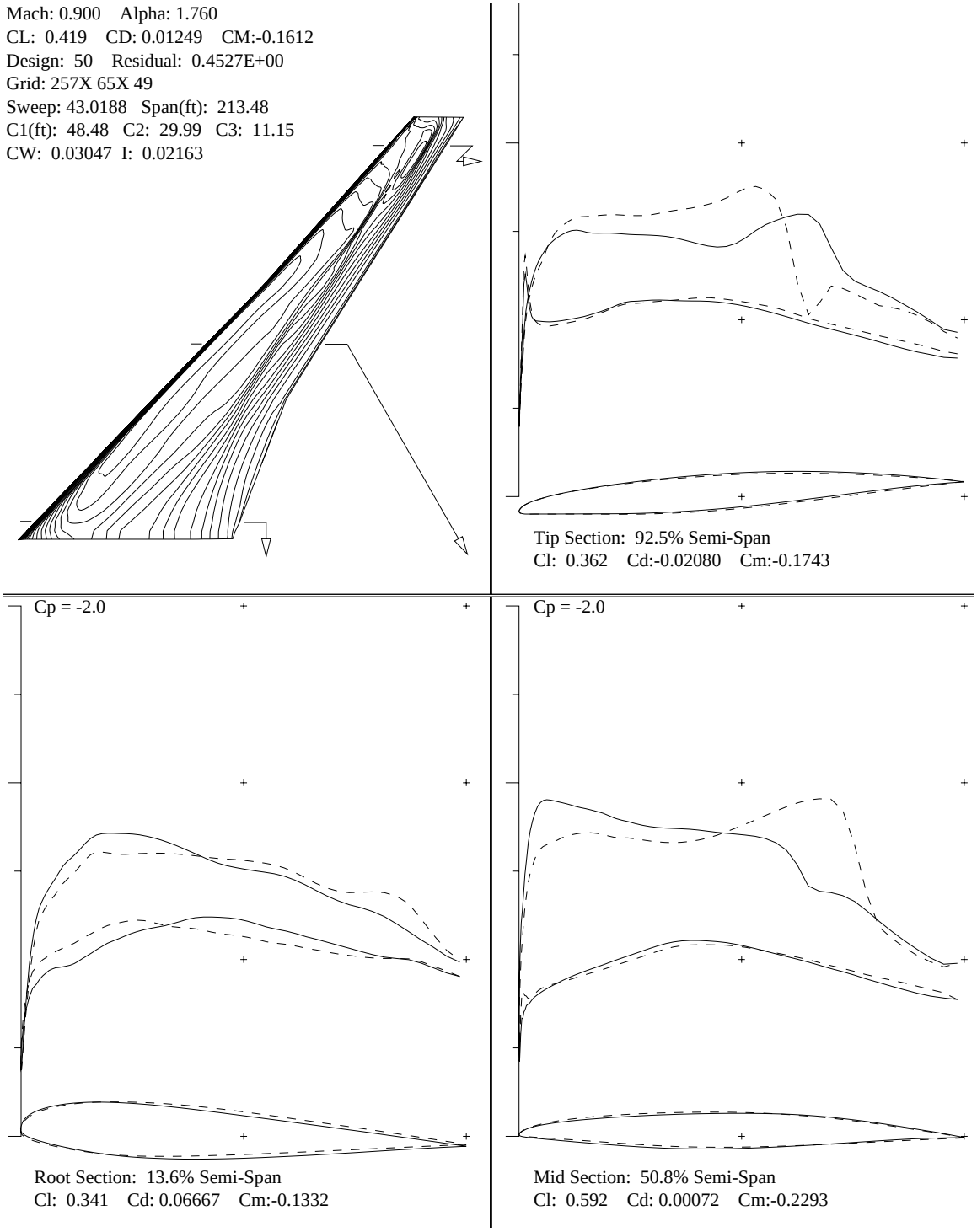

Figure 15. Redesign of Boeing 747, variable planform and maximizing range

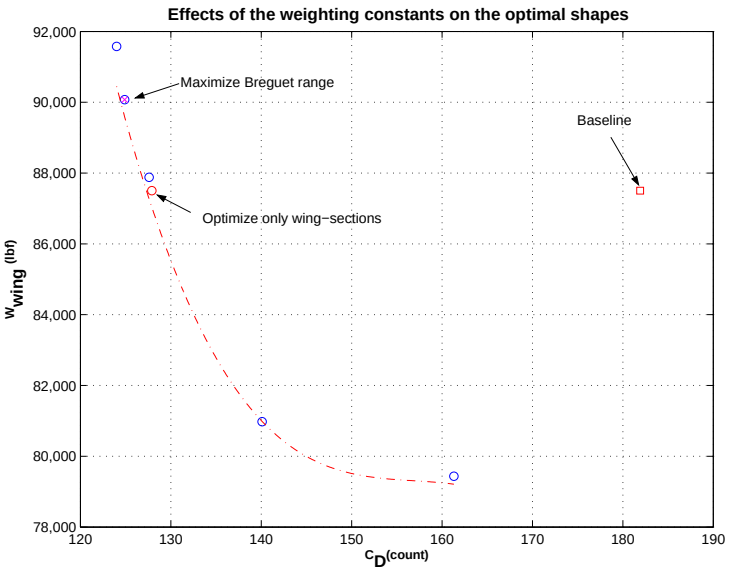

Figure 16. Pareto front of section and planform modifications

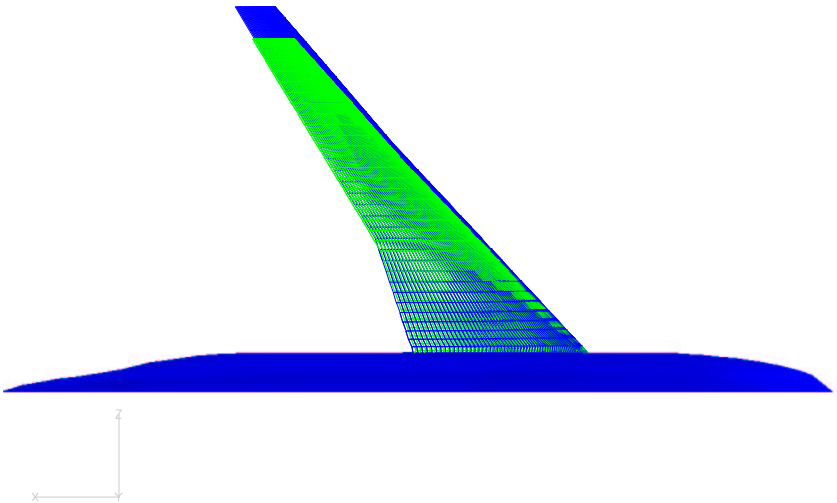

Figure 17. Superposition of the baseline geometry (green/light) and the optimized planform geometry (blue/dark), using α_1=1 and α_3=1

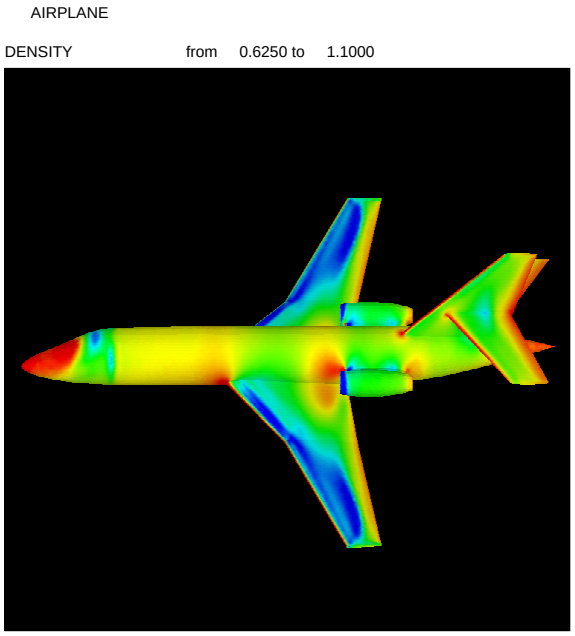

Figure 18. Density contours for a business jet at $M = 0.8$, $\alpha = 2$. Existing wing.

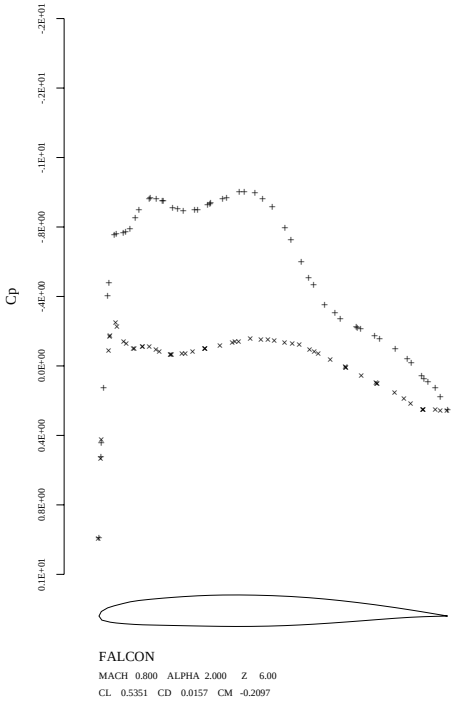

Figure 19. Pressure distribution at 66 % wing span

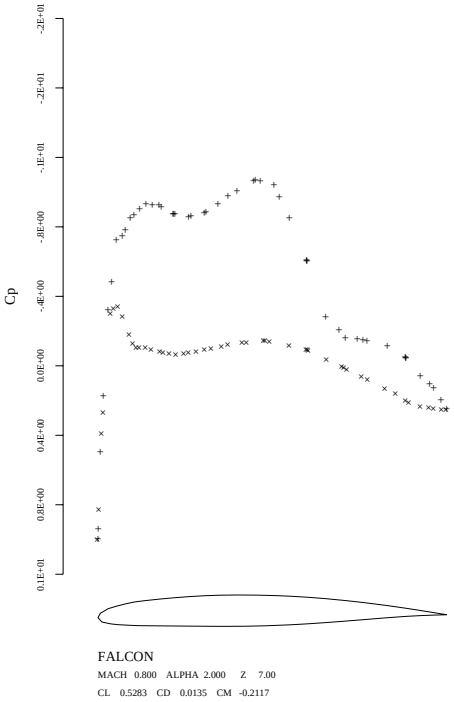

Figure 20. Pressure distribution at 77 % wing span

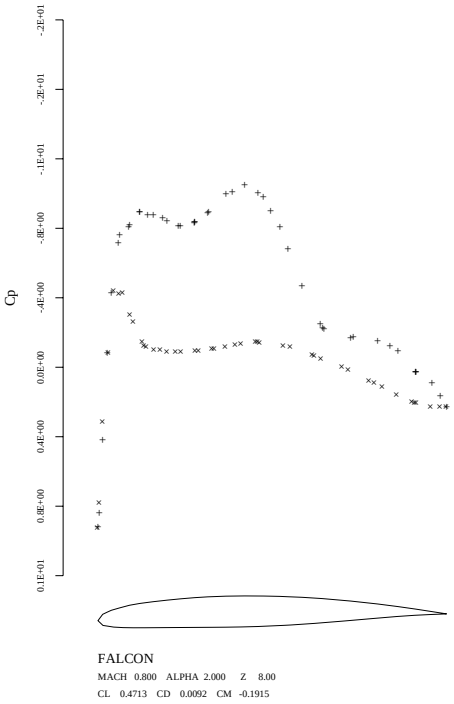

Figure 21. Pressure distribution at 88 % wing span

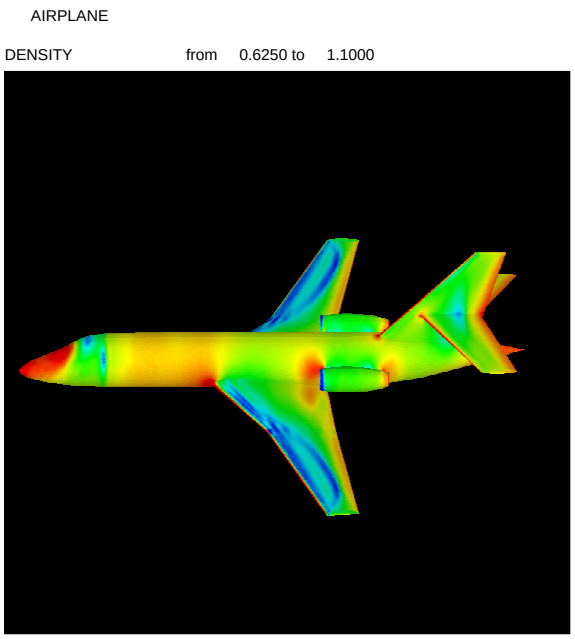

Figure 22. Density contours for a business jet at $M = 0.8$, $\alpha = 2.3$. After redesign.

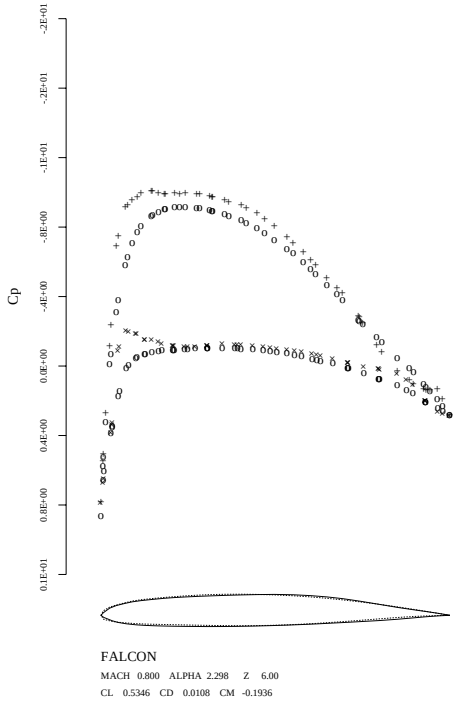

Figure 23. Pressure distribution at 66 % wing span, after redesign, Dashed line: original geometry, solid line: redesigned geometry

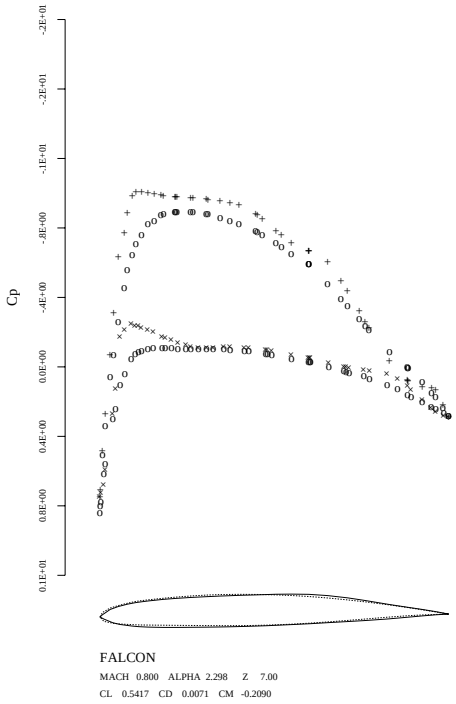

Figure 24. Pressure distribution at 77 % wing span, after redesign, Dashed line: original geometry, solid line: redesigned geometry

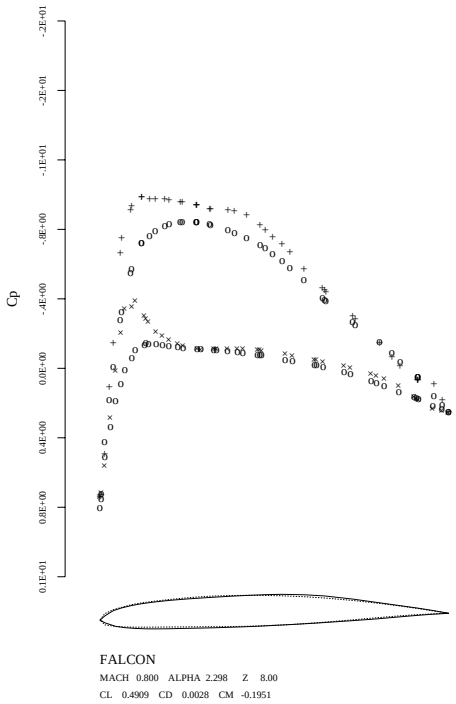

Figure 25. Pressure distribution at 88 % wing span, after redesign, Dashed line: original geometry, solid line: redesigned geometry